Philip Kargl, BSc

Application and sensitivity analysis of an electrochemical model for the simulation of lithium-ion transport in battery cells

Master's Thesis

to achieve the university degree of

Diplom-Ingenieur

Master's degree programme: Technische Physik

submitted to:

Graz University of Technology

Supervisor:

Assoc.Prof. Dipl.-Phys. Dr.rer.nat. Wolfgang Sprengel

Institute of Materials Physics

Graz, August 2016

Statutory Declaration

I declare that I have authored this thesis independently, that I have not used other than the declared sources/resources, and that I have explicitly marked all material which has been quoted either literally or by content from the used sources.

Graz, _____ _____

Date Signature

Eidesstattliche Erklärung[1]

Ich erkläre an Eides statt, dass ich die vorliegende Arbeit selbstständig verfasst, andere als die angegebenen Quellen/Hilfsmittel nicht benutzt, und die den benutzten Quellen wörtlich und inhaltlich entnommenen Stellen als solche kenntlich gemacht habe.

Graz, am _____ _____

Datum Unterschrift

[1] Beschluss der Curricula-Kommission für Bachelor-, Master- und Diplomstudien vom 10.11.2008; Genehmigung des Senates am 1.12.2008

Acknowledgement

First, I would like to thank my supervisor on the part of the Graz University of Technology, *Prof. Wolfgang Sprengel*, for his great support and his keen interest in the topic and the project.

Special thanks go to my supervisors at the VIRTUAL VEHICLE Research Center, *Mag. Franz Pichler* and *Dr. Martin Cifrain*, for their efforts to help me, for answering all my questions and for letting me participate in their expertise. I would also like to thank the whole battery group for their support and the nice working atmosphere.

The work reported in this thesis was partially funded by the Austrian Research Promotion Agency (FFG) within the "Energieforschung 2014" programme under the FFG-project No. 848773 and accomplished at the VIRTUAL VEHICLE Research Center in Graz. The author would like to acknowledge the financial support by the COMET K2 - Competence Centres for Excellent Technologies Programme of the Austrian Federal Ministry for Transport, Innovation and Technology (bmvit), the Austrian Federal Ministry of Science, Research and Economy (bmwfw), the FFG, the Province of Styria and the Styrian Business Promotion Agency (SFG). The author would also like to express his thanks to the supporting scientific project partner Austrian Institute of Technology GmbH (AIT).

Last but not least, I would like to say "Thank You" to my girlfriend Christina for her patience, her support, and for motivating me, when it was necessary and to my family for the moral and financial support.

Abstract

The effective storage of electric energy is an important issue in the 21st century, since the number of mobile electronic devices is vastly increasing and the electrification of individual transport has only just begun. An important approach is to store the energy electrochemically in batteries. Among the large variety of different cell chemistries, at this time the lithium-ion technology is seen to have the highest potential to power electric vehicles and electronic devices in the near future. For this reason, it is of vital importance to improve the capacity and the energy density of the cells. To be able to do this, a fundamental understanding of the transport processes for lithium-ions inside the cells is necessary. One possible way in order to investigate these processes is to set up a model which describes the different types of transport, and tries to simulate the cell behaviour. At the *VIRTUAL VEHICLE Research Center* such an electrochemical battery model whose governing equations describe the ion transport in the different regions of the cell has been developed. In this thesis, this model is applied to specific cell geometries. The influence of the physical parameters in the governing equations on the received results are investigated in detail. In contrary to other modelling approaches, in this model the cathode is described in full geometric detail. Different microstructures of the cathode, with different arrangements of the active material particles, are created. The model is applied to these geometries in order to reveal potential differences in the cell behaviour.

Kurzfassung

Die steigende Anzahl mobiler elektronischer Geräte, sowie die verstärkte Elektrifizierung von Fahrzeugen machen es dringend notwendig, die bestehenden Technologien zur Speicherung elektrischer Energie zu verbessern. Eine wichtige Rolle hierbei spielen Batterien. Von all den möglichen Zellchemien hat sich die Lithium-Ionen Technologie als besonders geeignet erwiesen, die aktuellen Anforderungen zu erfüllen. Dennoch ist eine stetige Verbesserung der Technologie unabdingbar, insbesondere eine Steigerung der Kapazität und der Energiedichte der verwendeten Elektrodenmaterialien. Dazu ist ein grundlegendes Verständnis der Transportmechanismen innerhalb der Zelle notwendig. Eine Möglichkeit diese Vorgänge im Inneren der Batterie zu untersuchen besteht darin, geeignete Modelle zu finden, mit denen versucht wird, das Verhalten der Zelle nachzubilden. Am *Kompetenzzentrum - Das virtuelle Fahrzeug* wurde solch ein elektrochemisches Modell entwickelt. Die Modellgleichungen beschreiben die Transportprozesse in den verschiedenen Bereichen der Zelle. In dieser Arbeit wird dieses Modell auf eigens erstellte Zellgeometrien angewandt. Im Gegensatz zu älteren Modellen, wird in diesem Modell die Kathodengeometrie im Detail dargestellt. Das Ziel ist es, erstens festzustellen, ob das Modell prinzipiell plausible Ergebnisse liefert, zweitens inwiefern eine Variation der im Modell verwendeten Parameter die Simulationsergebnisse beeinflusst und drittens zu untersuchen, welchen Einfluss die Anordnung der Aktivmaterialpartikel in der Kathode auf das Zellverhalten hat.

Contents

Abbreviations

BVE Butler-Volmer equation.

CS cycling stability.

DCC Discharge capacity.
DMC Dimethyl Carbonate.

EC Ethylene Carbonate.
ECDL Electrochemical double layer.
EOL End of Life.

GHG Green house gases.

LFP $LiFePO_4$.
Li Lithium.
LIB Lithium-Ion Battery.

NMC $Li(Ni_xMn_yCo_z)O_2$.

OCV Open Circuit Voltage.
OOM Order(s) of magnitude.

PC Propylene Carbonate.
PVDF polyvinylidene fluoride.

SEI Solid electrolyte interphase.

SS structural stability.

TMO transition metal oxide.

TS thermal stability.

List of Figures

1 Introduction

Energy has become and will remain one of the most important issues in global politics in the 21st century. The worldwide hunger for energy is on the rise. The International Energy Agency (IEA) predicted an increase in the world's energy demand of about one third by 2040 in their recent publication (*"World Energy Outlook 2015"*, *"WEO 2015 Special Report on Energy and Climate Change"* [1, 2]). Due to British Petrols *"Energy outlook 2035"* the rise will be about 37 % to 2035 [3]. The reasons for this development are manifold. On the one hand, there is the apparent increase of the world's population. The *United Nations* predict that up to 11.2 billion human beings will inhabit the earth by 2100 [4]. On the other hand, more and more electronic devices are used by an increasing number of people and, last but not least, humanities mobility is going up as well. According to the IEA [2] fossil fuels (coal, oil and gas) will remain the major energy carriers at the end of the period of consideration. In order to be able to guarantee the energy supply and to fulfil climate goals, the international community needs to focus on the use of renewable energies, like photovoltaic, wind energy etc.. Public sector entities finally have perceived the problem and introduced measures to tackle it. The *European Commission* for instance has set as their goals for 2030 to reduce the total emission of greenhouse gases (GHG) by at least 40 %, to rise the share of renewable energies to at least 27 % and to increase energy efficiency by at least 27 % [5]. In Austria the share of renewable energies is already at ca. 75 %, whereof the major part comes from hydro-power

[6]. Renewable energies (especially sun and wind) have the disadvantage that their supply is not as continuous and reliable as for conventional fossil energy carriers. It strongly depends on external conditions, like the weather, which are beyond human control. The excess electrical energy which is generated at peak times, has to be stored in some way, so it is available if required.

Concurrently to the increase in the share of renewables, the use of portable devices, such as smart phones, tablets or power tools as well as their energy demand, vastly increased over the last years which also raises the pressure for better energy storage technologies.
The intended reduction in GHG makes changes in the mobility sector inevitable, since in the European Union about 30 % of all primary energy (75 % of all oil) is consumed by transport and about 26 % of all GHG emissions are transport-related [7]. This share must urgently be reduced. The *European Road Transport Research Advisory Council (ERTRAC)* released a number of roadmaps ([7–9]) in the last couple of years, where they claimed their goals and visions for the mobility of the future. Possibilities in order to reduce the environmental impact of transport may be an efficiency increase for conventional internal combustion engines or, even more important, the enhanced use of electromobility, as for instance hybrid electric vehicles or battery electric vehicles. Especially the short- and medium-range transport in urban areas is well suited for electric vehicles, since the average mileage per day is below 100 km and the cars are only used 1-2 hours a day on average, so charging times will not be a major problem. The advantages of the electrification are clear. The air quality will get better, since the emission of CO_x and NO_x will decrease and also a major reduction of noise is expected. Of course the new mobility behaviour will require a corresponding infrastructure, such as a sufficient number of charging stations for instance.

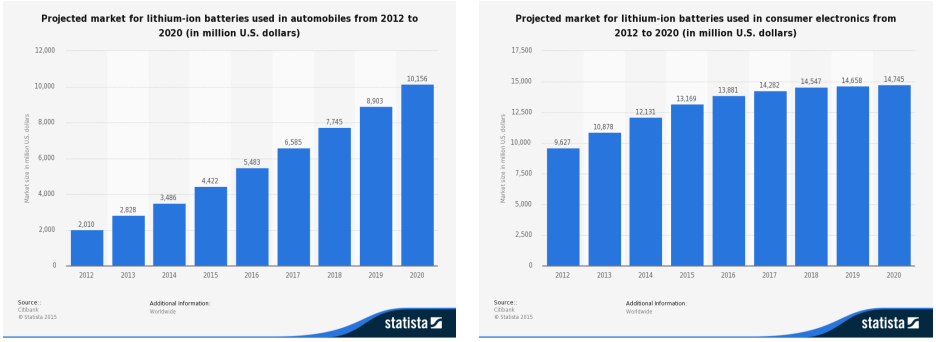

(a) (b)

Figure 1.1: ***a.)*** *Outlook on battery market* 2012 – 2020, ***b.)*** *Projected market for Consumer Electronics* 2012 – 2020 *([10, 11])*

All these issues show clearly that energy storage is vital and there is a high demand for better systems. From today's point of view, the best way to store energy is to do it electrochemically in batteries. They show a lot of flexibility concerning their applications, because of the high number of possible cell chemistries. Among all the potential chemistries, the lithium-ion technology has proven to excel other technologies in terms of capacity, energy density, cycle life etc. But there is still a long way to go for this technology to fulfil the future needs as well. Especially energy and power density, together with the capacity need to be improved. From an economic point of view it is expected that the worldwide market for lithium-ion batteries (LIB) for the use in automotive applications will strongly increase in the next years from about 2 billion US dollars in 2012, to more than 10 billion in 2020 [10], whereas the market for consumer electronics will saturate by 2020 [11]. The market size of electric vehicles is expected to increase from about 83 billion US dollars in 2012 to more than 270 billion in 2019 which corresponds to a growing rate of about 19 % per year [12]. The graphics are shown in Fig. 1.1.

An important step in the process of improving the performance and the

understanding of batteries is the set-up of suitable models that allow researchers to simulate battery behaviour. Such models can attribute different issues in the cell, as for instance the relevant transport mechanisms of the ions or thermal behaviour and, given that the results are reliable, make predictions for the behaviour of the cell for specific cases. This is an important matter in battery development, since a research group or a company does not need to build a prototype for every new approach which may save a significant amount of time and money.

At the *VIRTUAL VEHICLE Research Center* an innovative electrochemical battery model has been developed and the aim of this thesis is to apply this model to specific cell geometries.

As a preparation, the electrochemical aspects of LIB will be discussed in chapter 2. It covers the most important electrochemical basics, the fundamentals of LIBs, a short overview of possible cathode materials and already existing battery models, and the presentation of the electrochemical model used in this thesis. This model will be applied to specific cell geometries. In chapter 3 the simulation process will be explained in some more detail. It will be shown which cell geometries are used for the simulations, why they are used, and how they are created. The actual results of the performed simulations and their interpretation can be found in chapter 4. In chapter 5 a summary of the achieved results is given. A more detailed description of the content of the chapters 3 and 4 can be found at the beginning of each chapter.

2 Electrochemical Aspects of Lithium-Ion Batteries

In this chapter the most important electrochemical issues will be briefly presented (sections 2.1-2.3) in order to facilitate the understanding of the electrochemical battery model and the subsequent chapters. The introduction is based on the books *"Elektrochemie"* by Hamann and Vielstich ([13]) and *"Grundlagen der Elektrochemie"* by Schmickler ([14]). After the general introduction the fundamentals of LIBs will be explained in section 2.4. The cathode material is mainly responsible for the properties of the cell. Therefore, a more detailed view on possible cathode materials will be given in section 2.5, with a focus on transition metal oxides. A brief overview on different model types and some aspects of electrochemical battery models is given in section 2.6. At the end of the chapter, the electrochemical battery model which describes the transport mechanisms for the Li-ions in the cell and which has been developed at the *VIRTUAL VEHICLE Research Center*, will be presented in section 2.7. The governing equations will be explained, as well as the cell schematic which is a simplification of the real cell.

Schmickler defines electrochemistry in his book as follows:

> *"Electrochemistry is the science of the structure and processes at the phase boundary between an electronic conductor (the electrode) and an ionic conductor (the electrolyte) or the phase boundary between two electrolyte solutions ([14])."*

This short definition already contains the most important issues in electrochemistry. Such phase boundaries occur in electrochemical cells which are systems consisting of two electrodes separated by an electrolyte. An electrochemical cell is called a galvanic cell or a galvanic element if chemical energy which is stored in the active material of the electrodes, is directly converted into electrical energy in form of an electric current. Batteries are basically a set of galvanic cells which are connected in series or parallel.

There are many possibilities in designing a galvanic element. The electrodes can consist of a number of materials, for instance metals or oxides. The electrolyte is an ionic conductor and consists of a solvent and a salt which is dissolved into a number of positive and negative ions. The electrolyte itself is considered to be electroneutral, i.e. containing equal numbers of positive and negative ions:

$$\sum_i q_i \cdot c_i = 0 \tag{2.1}$$

where q_i is the ion charge of species i and c_i is the corresponding concentration. The sum of the charges over all species must yield zero. The electrolyte must be isolating for electrons. Otherwise, this would lead to a short circuit during cell operation. The properties of an electrolyte solution depend strongly on its ion concentration. In a dilute electrolyte, there is only a small number of dissolved ions and their mutual interaction can be neglected. This changes, when the ion concentration increases. Due to Coulomb interaction an ion is surrounded preferably by ions of the opposite charge. When such an ion wants to perform an electrochemical reaction, a

certain amount of energy is necessary to free itself of this ion shell and there will be less energy available for the actual reaction process. The single ion in a concentrated electrolyte is thus less reactive than in a dilute electrolyte. This loss of ion reactivity is considered by introducing an effective concentration which takes into account the energy loss due to ion-ion interaction. The quantity is called the **activity** a_i of a species i:

$$a_i = f_i \cdot c_i \tag{2.2}$$

where f_i is the activity coefficient. It is < 1 and takes the deviations from the interaction-free, ideal case into account. The higher the ion concentration in the electrolyte, the smaller f_i.

When a galvanic element is discharged, chemical reactions proceed in two spatially separated steps at the electrodes. The two steps can be summed up to an electro-neutral cell reaction formula. This cell reaction involves the positive and negative ions which are dissolved in the electrolyte and which get reduced or oxidised at the corresponding electrode. The electrode, where the oxidation occurs is called **anode**; the reduction process occurs at the **cathode**. There are two types of galvanic elements defined by the reversibility of the current producing cell reactions. If they are not reversible, the element can only be used once and is called a primary cell. In other systems the cell reactions are reversible and, when the active materials are used up, the cell can be recharged again. Such galvanic elements are called secondary cells.

When an electrode gets immersed into an electrolyte solution, a difference in the electrical potential between those two phases is established. To describe this phenomenon, the **chemical potential** $\mu_{c,i}$ of a species i is used:

$$\mu_{c,i} = \mu^0_{c,i} + RT\, ln\, a_i \tag{2.3}$$

It is defined as the potential energy of a system in order to perform chemical reactions or phase transitions. Here, $\mu^0_{c,i}$ is the chemical potential at standard conditions for temperature and pressure and is considered as constant, R denotes the gas constant, T is the temperature, and a_i is the activity as defined in Eq. 2.2. Two different phases are in equilibrium when their chemical potentials are equal for all involved species i. For the system electrode-electrolyte, directly after the immersion of the electrode, this condition will not be fulfilled and the system will thus not be in equilibrium. This leads to electrochemical reactions of the ions in both phases which tend to equalise the chemical potentials. The actual reactions depend on the system observed. For a metal electrode, such reactions may be for instance the reduction of positive ions and subsequent deposition at the electrode surface or the oxidation of neutral atoms in the electrode and their dissolution into the electrolyte. Depending on the actual values of the chemical potentials of the species i, one of these reactions will be stronger than the other. When the dissolution reaction prevails, there will be more positively charged ions in the electrolyte and the electrode will be more negatively charged due to the remaining electrons. When the deposition reaction is stronger, the conditions will be reversed. The result, however, is an inhomogeneous distribution of charges which is the reason for the difference in the electrical potential. This issue will be discussed in more detail in section 2.2. If this potential has reached a high enough value, the electrostatic forces acting on the ions are sufficient to prevent further reactions. So, the difference in electrical potential influences the equilibration process and thus has also to be taken into account. When treating charged species, it is therefore more practical to define the **electrochemical potential** μ_i:

$$\mu_i = \mu_{c,i} + z_i F \varphi = \mu^0_{c,i} + RT\, ln\, a_i + z_i F \varphi \tag{2.4}$$

where z_i is the charge of species i, F is the Faraday constant, and φ denotes

the established electrical potential which is also called **Galvani-potential**. The two phases will tend to reach equilibrium of the electrochemical potentials. In the further course of the calculations, the subindex c for the chemical potential at standard conditions will be omitted for convenience.

When now looking at a complete cell, there are two electrodes immersed into the electrolyte. There will be a difference in the Galvani-potentials between each electrode and the electrolyte which is called Galvani-voltage $\Delta\varphi$. Its dependence on the ion activity in the electrolyte will be derived in section 2.1. Its shape and the processes at the phase boundary electrode/electrolyte will be discussed in section 2.2. There is also a potential difference between the two electrodes which is called **cell voltage**. When there is no load on the cell which means that no net current is flowing, it is called **electromotive force** or **Open Circuit Voltage (OCV)**. In a galvanic cell, the cell voltage is reduced, when an electric current is flowing across an external circuit. How this happens in detail will be discussed in section 2.3.

2.1 Dependence of the Electrode Potential on the Activity

For the derivation of the Nernst equation, a so called metal-ion-electrode consisting of a metal M immersed into an electrolytic solution which contains ions M^{z+} of the same metal, is chosen as electrochemical system. The electrode reaction is of the following form:

$$M^{z+} + ze^{-} \rightleftharpoons M \tag{2.5}$$

An oxidised metal ion M^{z+} reacts with z electrons, gets reduced to an uncharged metal atom M and will be deposited at the electrode, or vice versa.

As it will be seen in section 2.4, the reactions in the electrodes in Lithium-ion batteries behave in a similar way. As mentioned above, equilibrium between the two phases is reached, when the electrochemical potential which was defined in Eq. 2.4, is the same for electrode and electrolyte. In this case it is the electrochemical equilibrium between the charged metal ions M^{z+} and the uncharged metal atoms M.

$$\mu_{M^{z+}} = \mu_M \tag{2.6}$$

$$\mu^0_{M^{z+}} + RT\, ln\, a_{M^{z+}} + zF\varphi_L = \mu^0_M + RT\, ln\, a_M + zF\varphi_M \tag{2.7}$$

The index M^{z+} denotes the metal ions in the electrolyte phase with the corresponding Galvani-potential φ_L, the index M denotes the metal atoms in the electrode, with the Galvani-potential φ_M. This can be mathematically solved for the potentials which results in an expression for the Galvani-voltage between the two investigated phases in equilibrium:

$$\Delta\varphi_0 = \varphi_M - \varphi_L = \frac{\mu^0_{M^{z+}} - \mu^0_M}{zF} + \frac{RT}{zF}\, ln\, \frac{a_{M^{z+}}}{a_M} \tag{2.8}$$

The first fraction containing the standard chemical potentials, can be summed up to the standard Galvani-voltage $\Delta\varphi_{00}$. The activity of the metal atoms in the electrode can be set to unity, because for neutral atoms the activity is obtained by the mole fraction χ_i of the species i:

$$\chi_i = \frac{n_i}{\sum_i n_i} \tag{2.9}$$

$$a_i = f_i \chi_i \tag{2.10}$$

here n_i is the amount of substance of the species i in mol. Since the metal atoms are the only species present in the electrode, their mole fraction has to be one. The activity coefficient for metal atoms not dissolved in an

electrolyte is one as well. For Eq. 2.8 the potential in the electrolyte is the reference point. For an arbitrary reference point, the equilibrium electrode potential φ_0 has to be written as follows:

$$\varphi_0 = \varphi_{00} + \frac{RT}{zF} \, ln \, a_{M^{z+}} \tag{2.11}$$

This Eq. 2.11 describes the dependence of φ_0 on the activity of the metal ions M^{z+} in the electrolyte and is called the **Nernst equation**.

2.2 Electrochemical Double Layers

As has been shown above, a difference in the electrical potential is established, when an electrode is immersed into an electrolyte. Electrochemical reactions, as can be seen in Eq. 2.5, will occur until the two phases have reached an equilibrium with respect to the electrochemical potential μ. Depending on whether the oxidation or the reduction reaction prevails, the electrode will get a negative or a positive charge. The electrolyte will then get a charge of the opposite sign. A space charge distribution at the interface between the two phases will be established and this phenomenon is called **electrochemical double layer (ECDL)**.

This issue will now be explained for a positively charged electrode surface. In the electrolyte, there are positive as well as negative ions. Due to the electrochemical reactions, there is a negative excess ion charge in the electrolyte and the electroneutrality condition in Eq. 2.1 is violated in the vicinity of an electrode. The negative ions in the electrolyte are surrounded by solvent molecules and try to get as close to the positively charged electrode as possible. The minimum distance between the electrode surface and the centres of charge of the ions is the radius r of the solvated negative ions. Near the

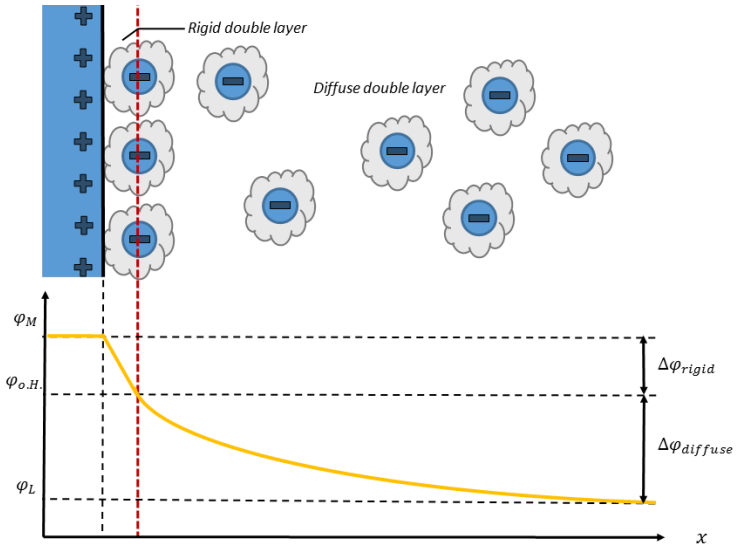

Figure 2.1: Schematic image of an electrochemical double layer with the corresponding potential values. In the rigid double layer there is a linear decrease in potential; in the diffuse double layer there is an exponential decrease. Based on Ref. 13

surface there will be two parallel layers of opposite charge. In Fig. 2.1 the situation is depicted. At the left-hand side there is the positively charged electrode. The excess negative ions with their solvate shells are located in the electrolyte. The red dashed line cuts through the centre of charge of these ions. It is called the **outer Helmholtz-plane** and the area between the two layers is called **rigid double layer** or **Helmholtz-layer**. This situation is very similar to a capacitor with a distance r between its plates. The progress of the electrical potential φ in this region can be described with the Poisson-equation. The problem can be considered as one-dimensional and with ρ being the charge density it takes the form of:

$$\frac{d^2\varphi}{dx^2} = -\frac{4\pi\rho}{\epsilon} \tag{2.12}$$

where ϵ is the permittivity of the medium. When the ions are assumed

to be point charges, the layer between the outer Helmholtz-plane and the electrode is charge-free which means a zero charge density in this region. Integration of the Poisson-equation then yields

$$\frac{d\varphi}{dx} = const. \tag{2.13}$$

meaning that the potential changes linearly with distance x in this region. The course of the potential with distance x from the electrode can be seen in the lower part of Fig. 2.1. The yellow line depicts the electrical potential. In the electrode itself it is constant at a value of φ_M and in the rigid double layer the linear decrease can be seen. If the distance to the electrode gets larger, the behaviour changes. The reason for this is that the strict arrangement of the ions cannot be preserved due to their thermal energy. The space charge gets more spread, as can be seen in the sketch. This region is called the **diffuse double layer**. After a longer mathematical derivation which will not be shown here, the change in the electrical potential turns out to be an exponential. The total difference in the potential between electrode and electrolyte is then the sum of the contributions of the rigid and the diffuse double layer.

$$\Delta\varphi = \Delta\varphi_{rigid} + \Delta\varphi_{diffuse} \tag{2.14}$$

The width of the diffuse double layer depends on the ion concentration in the electrolyte. If the concentration is high, the diffuse layer is considered as small and the total double layer can be approximated by the rigid layer alone. The interface then behaves like a capacitor.

2.3 Reaction Kinetics at the Interface between Electrode and Electrolyte

Up to this point the electrochemical systems were investigated in an equilibrium state with respect to their electrochemical potentials which means that there was no net current flow. The equilibrium state here is meant to be a dynamic equilibrium, so there are always electrochemical reactions, such as seen in Eq. 2.5, at the interface between electrode and electrolyte, but the forward and backward reaction are of the same magnitude and cancel each other out. When now a current is flowing, a cell is driven out of electrochemical equilibrium. A discharge current causes the cell voltage of a galvanic cell to decrease. This happens, because the potentials between the two electrodes and the electrolyte change. This difference of the electrode potentials with respect to their equilibrium values is called **overpotential** η.

$$\eta = \varphi - \varphi_0 \tag{2.15}$$

In an electrochemical cell different physical effects occur which are responsible for the change in the electrode potential with respect to a flowing current. Overpotentials occur, when an effect is limiting the discharge process or the ion transport. Such effects are for instance the charge transfer across the interface between electrode and electrolyte or the transport of species from the solution to the electrode surface or vice versa.

The charge transfer which happens with a finite velocity, as a limiting factor for the cell behaviour, is present in every galvanic cell and its contribution to the overpotential is thus inevitable. The magnitude of this charge transfer current across the interface is determined by the overpotential. The relation between these two quantities is an important issue in electrochemistry and will be derived in the following.

The derivation is based on Ref. [13] and starts with an dynamic equilibrium state $\varphi = \varphi_0$ at the electrode-electrolyte interface. If there is an overpotential at the electrode, either the forward reduction reaction or the backward oxidation reaction will be accelerated and the equilibrium is disturbed. There will be a net charge transfer across the interface with a corresponding electron current over the external circuit. The actual charge transfer can be described by the quantum-mechanical tunnel effect.

It is assumed that there is a high ion concentration in the electrolyte, so the behaviour of the double layer is similar to a capacitor (see section 2.2). When an external potential difference is applied to the cell, it shifts the potentials at the electrode to different values. Due to the relation $E_{el} = nF\varphi$, this causes also a shift in the electrical energy E_{el} of the ions in the vicinity of the interface. This energy shift can be explained with the **theory of the activated complex**. This means that the (electro-)chemical reaction proceeds by the formation of a meta-stable intermediate state with a higher energy. An energy barrier has to be surpassed both for the forward (cathodic) and the backward (anodic) reaction. This barrier is the difference in the free enthalpy ΔG between electrode and solution. For the electrochemical reaction this means that a change in the electrode potential from a value φ_1 to a value φ_2 reduces the energy barrier for one reaction direction and increases it for the other one. How the potential difference $\Delta\varphi$ exactly changes the energy barrier, depends on the species involved in the reaction however, it has to be in the range between zero and the full impact $nF\Delta\varphi$. To describe this situation, a so-called **charge transfer coefficient** α ($0 < \alpha < 1$) is introduced. For the anodic reaction (subscript $+$) this means:

$$\Delta G_+(\varphi_1) - \Delta G_+(\varphi_2) = \alpha nF\Delta\varphi \tag{2.16}$$

For the cathodic complementary reaction (subscript $-$) one can write

$$\Delta G_{-}(\varphi_1) - \Delta G_{-}(\varphi_2) = -(1-\alpha)nF\Delta\varphi \tag{2.17}$$

These two equations show that the charge transfer coefficients of anodic and cathodic reaction have to sum up to one, and that the barrier is increased for one direction and reduced for the other direction.

In the next step, an expression for the current density $j_{ct}^{\pm}$ of the anodic and the cathodic reaction will be derived. When the transport of species is assumed to be fast, the charge transfer (subscript ct) is the main limiting factor. The current density, in this case for the anodic reaction, can be written as the product of the particle current density J with the Faraday constant F and the number n of electrons participating in the reaction resulting in

$$j_{ct}^{+}(\varphi_2) = nFJ^{+}(\varphi_2) = nFc_{red}k_0^{*,+}exp\left(-\frac{\Delta G_{+}(\varphi_1) - \alpha nF\Delta\varphi}{RT}\right) \tag{2.18}$$

where c_{red} is the concentration of the reduced species and $k_0^{*,+}$ is the reaction constant. It contains the electron concentration in the electrode which is assumed to be constant due to the high mobility of the electrons. If now the value φ_1 is set as the origin of the potential, one can write

$$j_{ct}^{+}(\varphi) = nFc_{red}k_0^{+}exp\left(\frac{\alpha nF\varphi}{RT}\right) \tag{2.19}$$

The term $exp(-\Delta G_{+}(\varphi_1)/RT)$ has been included into the new reaction constant k_0^{+}. The same can be done for the cathodic reaction and results in

$$j_{ct}^{-}(\varphi) = nFc_{ox}k_0^{-}exp\left(-\frac{(1-\alpha)nF\varphi}{RT}\right) \tag{2.20}$$

with c_{ox} as concentration of the oxidised species. The Eqs. 2.19 and 2.20 must

also be valid for the equilibrium potential φ_0. In this case both equations are of the same value j_0, but with opposite sign. The variable j_0 is called **exchange current density** and describes the intensity of the reaction in the dynamic equilibrium. To introduce the overpotential η into the equations, one can write for the potential $\varphi = \varphi_0 + \eta$ which leads to the following equations:

$$j_{ct}^{+}(\varphi) = nFc_{red}k_0^{+}exp\left(\frac{\alpha nF\varphi_0}{RT} + \frac{\alpha nF\eta}{RT}\right) \tag{2.21}$$

$$j_{ct}^{-}(\varphi) = nFc_{ox}k_0^{-}exp\left(-\frac{(1-\alpha)nF\varphi_0}{RT} - \frac{(1-\alpha)nF\eta}{RT}\right) \tag{2.22}$$

The pre-factors and the exponential term containing φ_0 can be summed up to the exchange current density j_0. The total current density is the combination of the cathodic and anodic parts and leads to the so called **Butler-Volmer equation (BVE)** which describes the dependency of the electrical current density on the overpotential η:

$$j_{ct}(\eta) = j_{ct}^{+}(\eta) + j_{ct}^{-}(\eta) = j_0\left\{exp\left(\frac{\alpha nF\eta}{RT}\right) - exp\left(-\frac{(1-\alpha)nF\eta}{RT}\right)\right\} \tag{2.23}$$

The equation consists of two exponential terms with opposite sign. When the overpotential η goes to larger positive or negative values, one of those exponential terms will dominate and the other one will become negligibly small, resulting in an exponential behaviour of the current density j_{ct} for both large positive and negative η values. The factor α determines the impact of the reaction parts. If α is ~ 0.5 (which is indeed the case for most reactions) the reaction is symmetric. For $\alpha > 0.5$ the anodic part is steeper than the cathodic part, for $\alpha < 0.5$ the reverse is true.

2.4 Basics of Lithium-Ion Cells and Cell Set-up

Lithium-ion batteries (LIB) are currently a very widely used cell type. The reasons which are already brought up above, are, among others, their high energy and power density compared to other systems, e.g. the lead-acid or the nickel-metal-hydride battery. The first LIB has been developed by Akira Yoshino in the 1980s [15]. It was the first rechargeable battery system which reached a cell voltage of 3 V. At the moment LIBs are the only technology that can hold enough energy for the use in electric vehicles or current mobile electronic devices, such as smart phones or tablets. A classification of the different battery systems can be made according to the so-called Ragone-plot. An example for such a plot is given in Fig. 2.2. The axes are the specific energy and power. The first determines the amount of energy that can be stored per kilogram of the cell. The latter describes how fast the energy can be released from the cell. An ideal battery system would have a high value for both quantities and would be placed in the upper right corner of the plot. In reality only one of the values takes on a high value. In the plot it can be seen that LIBs have the highest energy density of the considered systems and can be designed in such a way that the specific power is increased, albeit this goes along with a reduction in specific energy.

A LIB, as well as other battery types, consists of two or more galvanic cells, connected either in series or parallel. When discharged, a battery directly converts chemical energy into electrical energy. In contrary to fuel cells, where the reactants are supplied from an external source, a battery is a closed system. The cell reactions in LIBs are highly reversible, so they rank among the secondary cells. During its operational life a cell underlies ageing and degradation phenomena such as irreversible capacity loss etc. The number of cycles which can be achieved until the end of life (EOL) criterion of the cell is reached, are in the range of 800-3000 cycles [17]. The

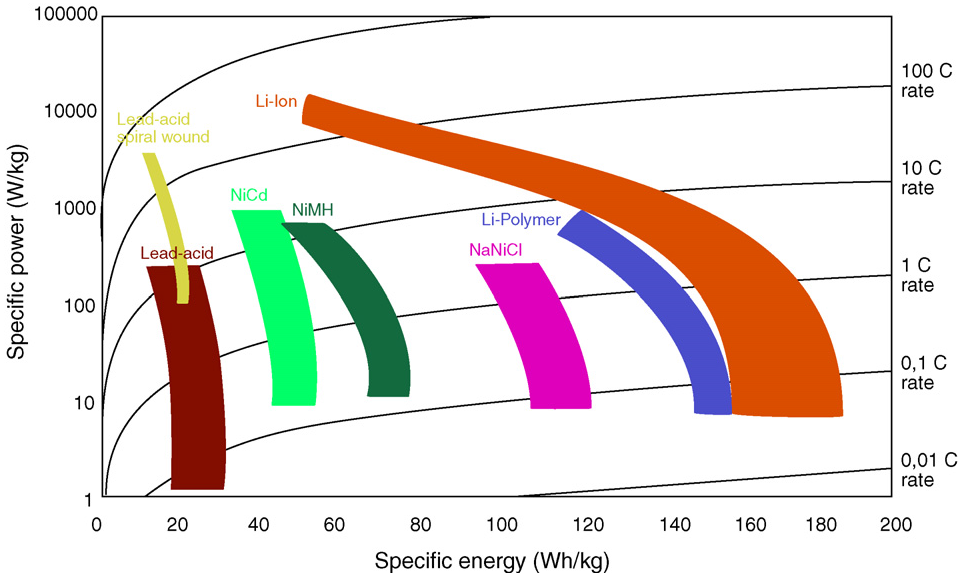

Figure 2.2: *Example of an Ragone-plot for the comparison of different battery systems regarding specific energy and specific power. The solid lines represent characteristic charge and discharge currents as depicted in the right. (According to Ref. 16)*

EOL of a battery is reached when the cell capacity drops below 80 % of its initial reversible value [18].

The basic building blocks for a battery are the same as for any other electrochemical cell: two electrodes with an electrolyte in between. Fig. 2.3 shows a schematic image of a LIB, containing all the relevant parts. At the left there is the current collector for the cathode (a.), made out of aluminium. It serves as electrically conducting connection between the electrodes and the external circuit. Adjacent to it, there is the cathode (b.). In the figure it is a layered transition metal oxide, where Li-ions get (de-)intercalated during battery operation. The cathode is a porous material soaked with an electrolyte. In between the two electrodes there is a separator (c.). It physically separates the two electrodes and is electronically isolating in order to prevent short-circuits. It has to be porous and must show a good wettability to the electrolyte, so ion transport through the pores of the separator is

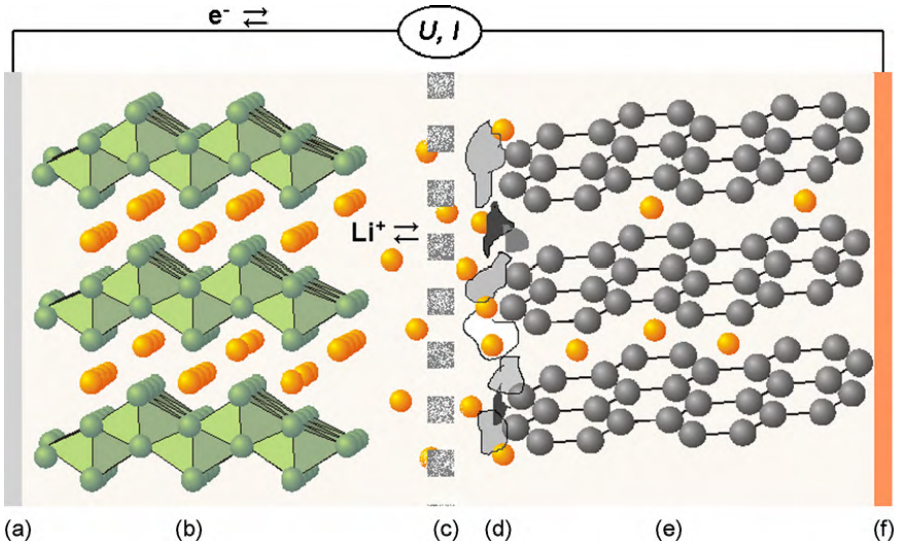

Figure 2.3: *Sketch of a Li-ion cell:* ***a.)*** *aluminium current collector,* ***b.)*** *cathode with a layered transition metal oxide as active material,* ***c.)*** *liquid electrolyte with porous separator,* ***d.)*** *solid electrolyte interphase layer,* ***e.)*** *anode with graphite as active material,* ***f.)*** *copper current collector. (According to Ref. 19)*

possible. It has to be electrochemically inert, mechanically stable and must not react with any active species in the cell. Materials used for separators are for instance membranes made out of microporous or non-woven organic materials, such as polyethylene or polypropylene [20]. Next to the separator at the anode, there is the so called "solid electrolyte interphase (SEI)" (d.). This denotes a phenomenon typical for LIB and will be explained in some more detail below. The anode (e.) in the cell schematics is made out of graphite which is a layered material as well and is the type of anode material which is widely used in LIBs. During battery operation Li-ions will get (de-)intercalacated, just as in the cathode. So in a LIB, in most cases, both electrodes are made out of intercalation materials, and the Li-ions get shifted from one electrode to the other when a current is flowing. At the right end of the figure, the copper anode side current collector is shown (f.). The schematics is completed by an external circuit connecting the two

current collectors.

For the cathode material mostly layered oxides are chosen. One widely used example is $LiCoO_2$. These and other possible materials are briefly discussed in section 2.5. The cathode, however, is not made out of the active material particles alone. A binder material, typically polyvinylidene fluoride (PVDF) is used in order to stick the particles together. To increase the electronic conductivity of the cathode, additives as for instance carbon black, are used [21]. Anodes are in most cases made of different modifications of graphite. Alternative anode materials are based on titianium oxides, for instance $Li_4Ti_5O_{12}$ which is used in commercially available cells [21].

Another critical part for LIBs is the electrolyte. Aqueous electrolytes cannot be used, because they are only stable up to a voltage of $\sim 1.5\,\mathrm{V}$. For higher voltages the electrolyte will get decomposed by an electrolysis process. Non-aqueous electrolyte solutions are electrochemically stable for much higher voltages and are thus suitable for the use in LIB. Another advantage is that they can be used at much lower temperatures than aqueous electrolytes. Their disadvantages are that they are more expensive, more toxic, flammable, and show a much lower conductivity than aqueous electrolytes [22]. Ingredients needed for a proper electrolyte are organic solvents and a Li-salt dissolved in them. Examples for organic solvents are dimethyl carbonate (DMC), ethylene carbonate (EC) or propylene carbonate (PC). As a salt mostly Lithium-Hexafluorophosphate $LiPF_6$ is in use which dissolves into Li^+ cations and PF_6^- anions.

As already depicted in Fig. 2.3, there is a special layer at the surface of the anode, the solid electrolyte interface layer (SEI). The occurrence of such a layer in non-aqueous battery systems has already been reported 1979 by Peled [23]. The reason for the appearance of this layer lies in the electrode potentials and the potential window, in which the organic electrolyte is

stable. For a common non-aqueous electrolyte, a stability window for the voltage from 0.8 V to 4.5 V versus a Li-electrode can be assumed [24]. If an electrolyte material operates at lower voltages, a reduction process occurs, when a current is flowing. If the voltage is above that window, an oxidation process appears. The cathode if for instance a transition metal oxide is used, has a potential which is below 4.5 V. A graphite anode, however, operates at a voltage below 0.8 V and is thus outside the stability window. When such a cell gets charged for the first time, a reduction process together with a degradation of the electrolyte at the anode takes place. The decomposed electrolyte components form the SEI. It acts like a solid electrolyte for the Li-ions and prevents the further decomposition of the electrolyte. The formation goes along with an initial irreversible capacity loss.

When the cell is discharged, the ions are deintercalated at the anode and move towards the cathode, where they are intercalated again. During charging this process is reversed. The charge or discharge current is often described in terms of the so called **C-rate**. When for instance a cell is discharged with a current of 1 C, the magnitude of the current is such that the initially fully charged cell would be completely discharged in one hour. A current of 2 C would mean a complete discharge in half an hour, 0.5 C would mean two hours etc.. An important quantity to characterise a LIB is the state of charge (SoC) of the cell. It is defined as the ratio between the amount of charge which is left in the cell and the maximum available capacity. It is given in % (a fully charged cell has a SoC value of 100 %). The SoC of a cell has a major influence on its behaviour.

A commercial LIB consists of a number of single cells which are connected in series or parallel. In Fig. 2.4 two ways of setting up a commercial battery are shown. The image to the right shows a prismatic cell, where the electrodes and the separator are stacked. The image to the left shows a cylindrical cell, where the electrodes and the separator are wound around a centre pin [25].

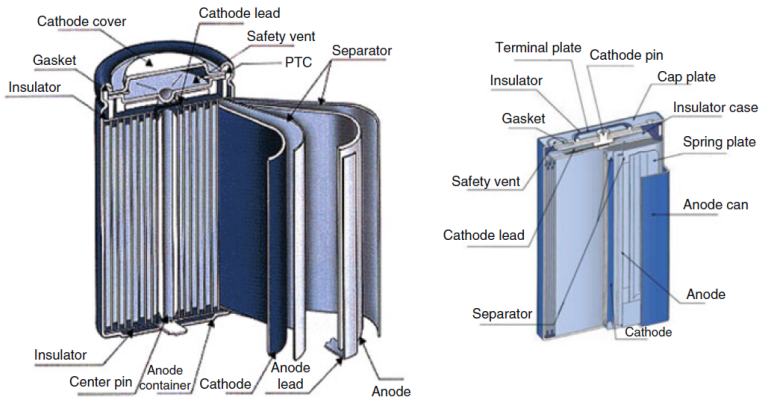

Figure 2.4: *Two possible realisations of commercial LIBs. To the right a prismatic cell is shown, were electrodes and separator are stacked. At the left hand side, a cylindrical cell is shown, where electrodes and separator are wound around a centre pin. (According to Ref. 25)*

To really have a working system, many other components are necessary, as can be seen in the figure.

2.5 Cathode Materials

Since important parameters of a LIB, as for instance the discharge capacity or the cell voltage, are mainly determined by the cathode material, it is essential for a further development to improve these materials or find alternatives to existing ones. In the following section a brief overview on possible candidates will be given, based on a review paper by Xu et al. from 2012 [26]. For further details the reader is referred to this reference. It is followed by a more detailed view on layered transition metal oxides (TMO), since they are the most common class for today's commercial LIB and the cathode material for the model cell which will be presented in chapter 3, is assumed to be of this type as well, namely $Li(Ni_xMn_yCo_z)O_2$ (NMC).

In the review by Xu et al. six material classes are considered. In Tab. 2.1 the most important features of each class are listed.

Besides TMO another group of materials used in commercial LIB are the **olivine compounds**. Their structural formula is $LiMPO_4$, where M denotes a metal, with the most prominent material being $LiFePO_4$ (LFP). Olivines excel because of their thermal and structural stability and their low costs. In addition, they are non-toxic and not harmful to the environment. Although their cycling performance is very good, their cell voltage is limited to about 3.3 V which in consequence lowers their energy density. Lithium diffusion in LFP is only one-dimensional which leads to a poor ionic conductivity. This, as a consequence, leads to a low rate capability which means that the cell cannot be cycled with high currents.

A material class very similar to the olivine compounds are the **tavorite compounds** which have Fluorine added which then writes as $LiMPO_4F$. The characteristics of this class are similar to the olivines. The extra fluorine atom leads to multidimensional lithium diffusion in contrary to the one-dimensional diffusion paths in olivines. The most investigated representative of this group is $LiVPO_4F$. This material has a very stable structure and thus a very stable cycling behaviour, with good capacity retention even at higher C-rates. Another advantage is the thermal stability at elevated temperatures. For this material a DCC of 140 mAh/g and voltages of about 4 V are possible. A disadvantage of this material class is the low energy density.

Spinel compounds with the structural formula LiM_2O_4 are considered as cathode materials as well. A prominent candidate of this material group, regarding its electrochemical behaviour, is $LiNi_{1/2}Mn_{3/2}O_4$. It shows a high upper voltage limit of 4.7 V which also leads to an acceptable reversible DCC of 140 mAh/g. A problem that naturally comes with the high voltage of the spinel compounds is the danger of electrolyte decomposition which

Table 2.1: Comparison of six different classes of cathode materials. *M* is a place holder for different metals. The most important advantages and disadvantages of each class are listed. (According to Ref. 26)

Type	Formula	Advantages	Disadvantages
TMO	$LiMO_2$	high theoretical DCC good CS good TS (without Co)	Co expensive, toxic environmentally problematic not all Li can be extracted
NMC	$Li(Ni_xMn_yCo_z)O_2$	high DCC , good CS good TS (without Co)	see TMO
Olivines	$LiMPO_4$	good SS, CS and TS safe material, non-toxic environmentally friendly	low voltages, low DCC low κ 1D Li diffusion
Tavorites	$LiMPO_4F$	similar to olivines faster Li diffusion	low energy density not investigated well enough
Spinels	LiM_2O_4	high voltage and energy density good SS and CS	rather low DCC electrolyte decomposition
Silicates	Li_2MSiO_4	very high theoretical DCC good at elevated temperatures	practical DCC much lower low SS and CS low κ (without coating)
Borates	$LiMBO_3$	light structural unit $\rightarrow$ high energy density	poor electrochemical performance not investigated well enough

Abbreviations: *TMO ... transition metal oxides, DCC ... discharge capacity, SS ... structural stability, TS ... thermal stability , CS ... cycling stability, κ ... ionic conductivity, ec ... electrochemical*

leads to cycling instability.

A relatively new material class for LIB cathodes are the **silicate compounds**. Their structural formula is Li_2MSiO_4. For these materials two lithium ions per structural unit can theoretically be extracted which would lead to a very high DCC of $\sim 300\,\mathrm{mAh/g}$ in theory. Lithium diffusion goes along two-dimensional paths in this material class. Examples for materials of this group are Li_2FeSiO_4 and Li_2MnSiO_4. For both materials, however, not even half of the high DCC as predicted in theory could be achieved which means an effective extraction of less than one Li-ion per structural unit. Reasons for this poor electrochemical behaviour are the low conductivity of these materials in general, and structural instabilities during cycling. The performance could be improved by carbon coating of the particles.

A group of materials which is interesting because of its very light structural unit, are the **borate compounds** $LiMBO_3$. These materials show a high theoretical energy density which has not yet been achieved in practice. They are very sensitive to moisture in the air which drastically deteriorates their behaviour. This kind of material has only been considered recently and up to now they perform worse than other cathode materials.

In the next section the transition metal oxides and especially NMC will be treated in more detail.

Transition Metal Oxides

As mentioned above lithium transition metal oxides are the most common cathode materials. They exhibit the structural formula $LiMO_2$, where M represents a 3d transition metal like cobalt, nickel, manganese and combinations of them. Due to the definition of the *International Union of Pure and Applied Chemistry (IUPAC)* a transition metal is "an element whose atom

has an incomplete d sub-shell, or which can give rise to cations with an incomplete d sub-shell [27]." Their layered structure suits well for intercalation of Li. The most prominent material of this group for the last decades has been $LiCoO_2$. It was the first cathode material considered for LIB and introduced in 1980 by the group of JB Goodenough [28]. This material shows a high theoretical capacity of 274 mAh/g, but due to structural instability of the compound, when more than half of the Li is extracted, the actually achievable capacity is only about 140 mAh/g. A further disadvantage of this material is the fact that the natural abundance of cobalt is fairly low which makes it a quite expensive material. If the number of electric vehicles increases, problems in providing enough cobalt for building the necessary batteries will probably occur. In addition to this shortages, Cobalt is poisonous and problematic for reasons of environmental protection.

All these problems show the necessity for alternative materials which on the one hand need to have a higher reversible discharge capacity and on the other hand are at lower costs and safer than $LiCoO_2$. Over the time many possible candidates were developed, as for instance $LiNiO_2$, $LiMnO_2$ which avoid the use of Cobalt but suffer from stability problems. Combinations of these metals, like $Li(Ni_xMn_y)O_2$ with different compositions have also been investigated to replace $LiCoO_2$.

One of the most promising candidates for a new cathode material however is $Li(Ni_xMn_yCo_z)O_2$ (NMC), a combination of all three transition metals mentioned above. It is the cathode material which will be used in the test cell for the simulations of the present work. It has been developed about since the turn of the millennium and has performed quite well. The first NMC type which has been developed was $Li(Ni_{1/3}Mn_{1/3}Co_{1/3})O_2$ [29–33]. Investigations with different measuring techniques revealed the structure to be of the α-$NaFeO_2$-type with the space group $R\bar{3}m$ and a hexagonal lattice. The oxygen sublattice is distorted from the face-centered cubic lattice in the

direction of the hexagonal c axis. This corresponds to a layered structure as it has been found for $LiCoO_2$ and other compositions of NMC as well. It enables a fast two-dimensional diffusion and a high capacity in theory [34].

Two possible structural models for $Li(Ni_{1/3}Mn_{1/3}Co_{1/3})O_2$ have been investigated by Koyama et al. [30]. The first one is called the *superlattice model*. Here the structure is built up by $(Ni_{1/3}Mn_{1/3}Co_{1/3})O_2$ slabs which alternate with Li slabs. They show the $[\sqrt{3}x\sqrt{3}]R30^\circ$ superlattice or superstructure in Wood's notation. A superstructure in solid-state physics is an additional periodic structure which has a bigger unit-cell than the crystal itself. Wood's notation describes the superstructure in terms of the regular lattice. The above term means that the superstructure is $\sqrt{3}$ units long in x- and y-direction and rotated by an angle of 30°. For further crystallographic details the reader is referred for instance to the book *Surface Science: An introduction* by Oura et al. [35]. The second model was called the *piled-up model* and here it is assumed that slabs of CoO_2, NiO_2 and MnO_2 are piled up alternating with Li slabs. Realizations of these structures can be seen in Fig. 2.5 The two models are seen as two extreme cases. The formation energies of both structures were calculated and the superlattice structure was determined to be the energetically favourable one. Another result of the investigations was that the volume decrease due to a decreasing amount of Li in the structure for the investigated NMC is smaller than for other transition metal oxides.

$Li(Ni_{1/3}Mn_{1/3}Co_{1/3})O_2$ is not the only possible realization of NMC, so research has also be done for other compositions of this material. Noh et al. investigated the structural and electrochemical performance of NMC with increasing Ni content from 1/3 to 0.85 [36]. The α-$NaFeO_2$ structure was confirmed also in that report by X-ray diffraction. The investigations showed that the average particle size decreases with increasing Ni content.

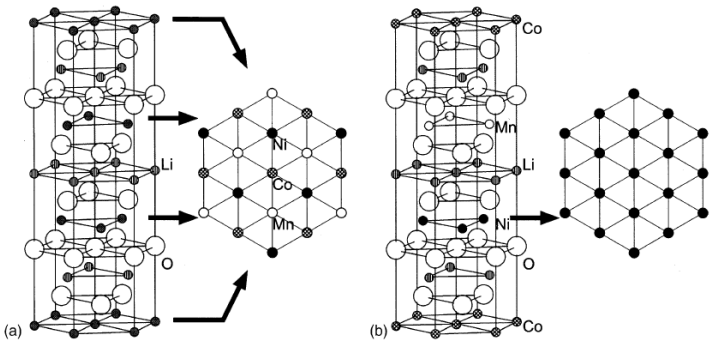

Figure 2.5: Two possible structures for $Li(Ni_{1/3}Mn_{1/3}Co_{1/3})O_2$ proposed in Ref. 30. (a) is the superlattice model, (b) is the piled-up model. Both show a layered structure.

Coin cells with NMC cathodes and Li metal anodes were built and cycling of the cells showed that the initial DCC increased with increasing Ni content, as well as the ionic conductivity. But on the other side, cells with Ni-rich cathodes showed a much worse cycling behaviour (about 50 % capacity fade after 100 cycles) which indicates a low structural stability. An additional effect was that a high amount of Ni leads to an increase in the volume of the unit cell of NMC. The reason for these effect is assumed to be a phase transformation of particles on the surface to a spinel-like structure.

A phenomenon that has been reported frequently is the so-called *cation-mixing*. This means that Ni, Mn or Co ions do not reside in their layer, but change place with Li-ions. This mixing behaviour has been investigated by Yan et al. among others for different compositions of NMC [34]. Transmission electron microscopy measurements have shown that Co and Mn mainly stay within their layers, whereas Ni shows a much higher degree of mixing. A reason for this may be that the Ni ions have a similar size than the Li-ions. It is not yet clear if this cation mixing has a positive or negative effect on the cell behaviour.

2.6 Modelling of Batteries

The necessity of understanding the physical and chemical processes which are responsible for the performance of an electrochemical cell or a battery is as old as batteries itself. Therefore, a lot of effort has been made over the last decades in order to develop and improve accurate mathematical models which allow to reproduce the electrochemical behaviour of batteries. There are many different cell chemistries, reaching from the classical lead-acid cell to modern high power Li-ion cells. Although the basic principles are the same in every electrochemical cell, there are specific features for each chemistry which have to be attributed in a model.

2.6.1 Model Types

The following brief overview of different model types is based on the book *"Automotive Battery Technology"* [37] from 2014 and on a review paper by Ramadesigan et al. [38] from 2012.

There are different approaches in trying to simulate cell behaviour, depending on the desired results. A detailed description would go far beyond the scope of this thesis, so in this section only a brief overview of existing model types will be given. The first attempts that have been made are called **Empirical models** or **Black-box models**. They mostly consist of only one single equation with a given model order and try to match a measured phenomenon as good as possible. Such models do not consider any physical or chemical properties and give no insight in the processes inside the cell. An advantage of these models are their simplicity and, in further consequence, their calculation speed.

Another way of simulating batteries is by using an **Equivalent Circuit Model**. Observations have shown that the behaviour of a cell is similar to an electrical circuit consisting of resistances and capacitors, so the models are also called **RC-models**. The model consists of a voltage source which represents the OCV of a cell, an inner resistance which simulates an initial voltage drop, when a current is applied, and a certain number of RC circuits which are used to model the dynamic behaviour of the cell. In a way, RC-models are empirical models as well, since they give no insight into internal battery processes. But in contrary to the Black-box models, they in a way refer to the cell structure. Current RC-models are fast and only need a small number of parameters. An overview of the equivalent circuit models used in literature can be found in Ref. 39.

These first two examples of possible models do not refer to physical processes inside the cell. A study of these processes requires more complex models which directly describe the microscopic charge transport mechanisms. Such models are called **Electrochemical models**. Due to their complexity, many parameters are needed which makes the evaluation more difficult. A very brief overview of existing electrochemical battery models is given in the following section.

2.6.2 A brief Overview of Electrochemical Battery Models

Electrochemical battery models directly refer to transport processes inside electrodes and electrolyte. The primary processes are diffusion due to concentration gradients and migration of charged particles due to electric fields. Another process which can occur in a liquid electrolyte phase is convection which is the collective movement of particles in a fluid. This model type is computationally expensive, but it gives much more insight into the cell physics.

LIBs were commercially not available before the 1990s. The basic framework of electrochemical battery modelling, however, is much older and has been developed since the 1960s for other systems, such as the lead-acid battery. An important contribution was made by John Newman and his co-workers. They developed equations describing the behaviour of porous electrodes, at first in general [40, 41] and later adapted for battery applications [42]. Although much development has been done over the past decades, the original equations, with some adaptations, are basically still in use.

In the model developed by Newman [42], a porous electrode consists of a solid, porous matrix, with a metal contact on the one side, and an electrolytic solution on the other side. The pores of the matrix are filled with the solution. The exact micro-geometry is not considered, instead the electrode was assumed to be a superposition of the solid and the electrolyte phase. An overall porosity of the electrode is defined which is used as a scaling factor for model parameters such as the electronic and ionic conductivities which are thus seen as effective values. The electrolyte itself is a concentrated binary electrolyte which means that one single salt is dissolved in a solvent and that the ion concentration is high. In total there are three species present: anion, cation and solvent molecules.

As a result of the considerations made, Newman defines governing equations for the model. A part of them is based on Ohm's law and describes the current in the matrix and in the solution phase. The current is caused by gradients in the ion concentration and the electrical potential. Another important assumption in Newman's model is electroneutrality for each phase, as defined in Eq. 2.1. This means that the number of positive charges must equal the number of negative charges. A requirement for this to hold is that the ECDLs at the phase boundaries between matrix and solution are considered very small compared to the other phases. The last building block in the model describes the charge transfer across the interface solid

matrix/solution and is based on the BVE as described in Eq. 2.23.

A model for a Li-cell that is able to simulate its charge and discharge behaviour, has been developed by Doyle [43, 44], a co-worker of Newman. His cell consists of a Li metal anode and a intercalation cathode with a solid polymer electrolyte in between. The anode is considered as a Li-source and the focus of the model is set on the processes inside the cathode and in the electrolyte. For simplification, one-dimensional transport through the cell is assumed and effects, as for instance the SEI formation at the interface between the anode and the electrolyte, as well as volume changes are neglected. The author uses concentrated solution theory, because in LIBs, the electrolytes usually are highly concentrated. In contrary to dilute solution theory, the ions interact with each other. Instead of the concentrations c_i the activities a_i, as defined in Eq. 2.2, are used. As the driving force for mass transport the gradient in the electrochemical potential is assumed. Doyle's model was adapted and applied on a dual insertion Li-ion cell [45], consisting of a graphite Li_xC_6 anode and a $Li_yMn_2O_4$ cathode, separated by a polymer electrolyte. Since the anode in this model is an insertion electrode as well, transport phenomena have to be investigated for three regions. The same basic equations can be used for both anode and cathode if the different properties of the electrodes are considered.

Latz et al [46, 47] derived a model for the transport of ions, charge and heat in Li-ion insertion batteries directly from thermodynamic principles. Again, convective transport is neglected, and a binary electrolyte is assumed, as well as electrocneutrality. The model derivation has its origin in the fundamental thermodynamic relation which describes how the internal energy density can be changed in the system. Equations for the conservation of Li-ions, charge and entropy are set up. In combination with Maxwell's equations expressions for the fluxes (mass, charge, heat) are derived. Driving forces for these fluxes are a concentration gradient, an electrical field and a

temperature gradient.

Another approach for developing an electrochemical battery model has been made by Smith et al. [48]. His model describes a cell consisting of two porous insertion electrodes (anode: graphite, cathode : metal-oxide) with a separator in between. For deriving the governing equations for transport of species, again porous electrode theory and concentrated solution theory are used. The independent variables in the governing equations are the concentration at the interface of electrolyte and solid, and the potentials in solid and electrolyte. The variables are coupled by a BVE. The model results in a voltage response to an input current.

This brief overview only displays a small part of the wide field of battery modelling, since a more complete review would go far beyond the scope of this thesis. In the next chapter the model developed in this project will be described in detail.

2.7 The Electrochemical Battery Model used for the Simulations

After a short review on the most important electrochemical issues and battery modelling, the model used in this thesis will now be defined. The model was developed by the *VIRTUAL VEHICLE Research Center* and covers the important physical effects which play a role in the battery cell. It describes the transport mechanisms for Li-ions both in the electrolyte and in the particles, as well as the reaction kinetics at the interface between these two regions.

The specifications for the model cell used in this thesis differ from the general cell shown in Fig. 2.3. The specifications and differences are as

follows:

- The anode is metallic lithium and is not modelled in detail.
- The cathode consists of NMC.
- The electrolyte is a mixture of the solvents EC and DMC with the Li-salt $LiPF_6$.
- A simplified cell schematic was defined which separates the cell into regions, where the different governing equations hold. The resulting sketch is shown in Fig. 2.6.

The cell is separated into three basic parts: anode, separator and cathode. From the modelling aspect two regions are defined: electrolyte, denoted by Ω_L and cathode particles, denoted by Ω_S. At the right side, shown in grey, there is the Li-metal anode. The blue region is the electrolyte (Ω_L). The yellow spheres are the active material particles in the cathode (Ω_S). The dashed black line marks the boundary between separator and cathode. The anode is modelled as a plane, where Li-ions can transfer across the interface Γ_{Li} between anode and electrolyte (Ω_L). Ion transport in the anode is not part of the model. The separator in the schematic is no separate region; it is considered to be electrolyte and is thus described with the same set of equations. The cathode consists of a number of particles, embedded in electrolyte. The Li-ions get transferred across the interface between electrolyte and particles Γ_{LS}. In contrary to the model developed by Newman [42] which scaled the properties of the cathode with a porosity parameter, here the cathode is modelled in full geometric detail. However, the exact geometry of the separator is not modelled in detail, but instead Newman's approach is used and the porosity of the separator is considered by scaling the electrolyte properties, such as the conductivity and the capacity.

In the model the assumption is made that the electronic conduction in the particles is very fast compared to the ionic conduction and that all the

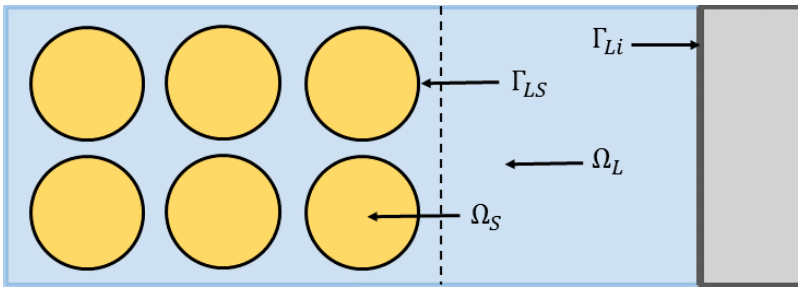

Figure 2.6: Schematic image of the cell used in the model. The grey area is the anode, with the interface Γ_{Li} to the electrolyte Ω_L. Left of the anode is the separator. The dashed line marks the transition to the cathode with the active material particles inside in yellow (Ω_S). Γ_{LS} is the interface between particles and electrolyte.

particles in the cathode are electrically connected, although this connection cannot be seen directly in the geometry. Therefore, all particles are on the same electrical potential which is why the electronic transport in the particles is not modelled and the electrical potential in the particles is not considered as an independent variable. When the electrochemical reaction at the interface is completed, the electron is not considered further. For the same reasons, the current collectors are not part of the model. The electroneutrality condition defined in Eq. 2.1 which is also used by Newman [42], is assumed in this model as well. In total, there are three independent variables in the model:

1. the Li-ion concentration inside the particles denoted c_s
2. the Li-ion concentration inside the electrolyte denoted c_l
3. the electrical potential in the electrolyte, ϕ_l

The derivation of the governing equations was not part of this thesis and therefore only the final governing equations will be briefly presented.

The Li-ion transport in the particles of the cathode is modelled with a diffusion equation, where the driving force is a gradient in the Li-ion

concentration in the particles c_s:

$$\frac{\partial c_s}{\partial t} - \nabla \cdot (D_s \nabla c_s)) = 0 \quad \text{in } \Omega_S \tag{2.24}$$

where D_s is the diffusion coefficient with the unit $\mathrm{m^2\,s^{-1}}$ which sets the velocity of the diffusion process. It is assumed to be SoC dependent in the model and is thus written as a product $D_s = D_0 \cdot D_s^*(SoC)$, where D_0 sets the order of magnitude (OOM) and D_s^* is SoC dependent, non-linear and defines the actual value. It has to be noted that the scaling factor D_0 used in this equation is not the same as the pre-factor in the Arrhenius-equation which is used to describe the temperature dependence of diffusion in solid materials.

The ion transport in the electrolyte is based on the Poisson-Nernst-Planck equations which describe ion transport in media, where a concentration gradient ∇c_l and a electrical potential gradientv $\nabla \phi_l$ are present:

$$\frac{\partial c_l}{\partial t} - \nabla \cdot (\frac{RTt_1}{F^2}\frac{\kappa(c_l)}{c_l}\nabla c_l + \frac{t_1 \kappa(c_l)}{F}\nabla \phi_l) = 0 \qquad \text{in } \Omega_L \tag{2.25}$$

$$- \nabla \cdot (\frac{RT}{F}(2t_1 - 1)\frac{\kappa(c_l)}{c_l}\nabla c_l + \kappa(c_l)\nabla \phi_l) = 0 \quad \text{in } \Omega_L \tag{2.26}$$

where κ is the ionic conductivity in the electrolyte, and t_1 is the transference number for Li-ions which describes the share of the Li-ion current with respect to the total current which in this case includes the contributions of all ions present in the electrolyte. The first Eq. 2.25 can be seen as an extended diffusion equation with an additional gradient in the electrical potential. The second Eq. 2.26 is derived from the electroneutrality condition.

Another important part in describing the transport is the charge transfer across the two interfaces Γ_{LS} and Γ_{Li}. The equation used in the model is

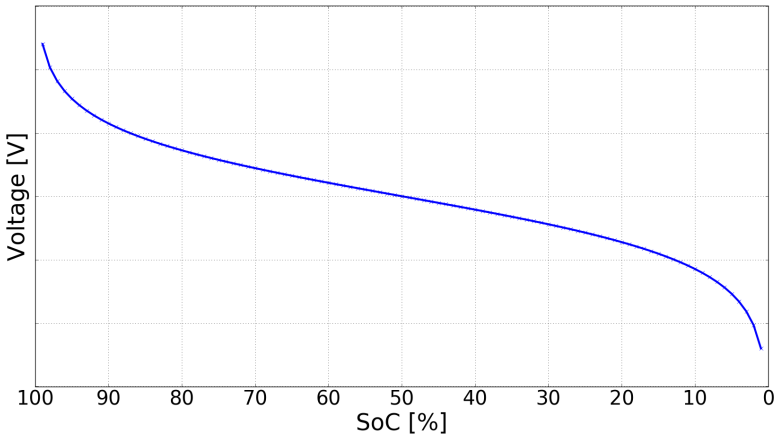

Figure 2.7: *Example of an OCV curve for a cell with an NMC cathode and a Li-metal anode. The x-axis is the SoC of the cell. The value of the OCV is higher when the cell is fully charged and decreases for smaller SoC values.*

based on the BVE, as already described in section 2.3:

$$j_{BV} = i_0\left(\frac{c_l}{c_{l0}} exp\left(-\frac{\alpha F}{RT}\eta\right) - exp\left(\frac{(1-\alpha)F}{RT}\eta\right)\right) \qquad \text{at } \Gamma_{LS} \tag{2.27}$$

$$j_{Li} = k_{Li}\left(\frac{c_l}{c_{l0}} exp\left(-\frac{\alpha F}{RT}\eta_{Li}\right) - exp\left(\frac{(1-\alpha)F}{RT}\eta_{Li}\right)\right) \qquad \text{at } \Gamma_{Li} \tag{2.28}$$

The exchange current density i_0 is also SoC dependent and can be written as a product $i_0 = k_{BV} \cdot i_0^*(SoC)$, with k_{BV} being a dimensionless reaction constant setting the OOM, and $i_0^*(SoC)$ defining the SoC dependent part with the unit $\mathrm{A\,m^{-2}}$. The overpotential for the cathode takes the form

$$\eta = \phi_s - \phi_l - U_{ocv} \tag{2.29}$$

where U_{ocv} denotes the value of the OCV. For the Li-metal anode there is no SoC dependence in the pre-factor of the BVE k_{Li}. The dynamic equilibrium does not change with the SoC. It is assumed that the anode is an infinite reservoir for Li-ions. In order to solve the system of governing equations a

number of boundary and intitial conditions has to be stated which describe the behaviour of the system at the beginning of the simulation and at the boundaries.

When one takes a look at the equations, it can be seen that the SoC plays a major role in the model. The SoC of the cell has a direct influence on D_s^*, i_0^* and on the OCV. As an example an OCV curve in dependence of the SoC for the modelled cell is given in Fig. 2.7. It can be seen that a fully charged cell has a high OCV value. The value decreases with decreasing SoC. Whereas the OCV has a smaller slope for medium values of the SoC, it gets bigger when the cell is nearly fully charged or nearly empty. This causes the cell to show a different behaviour when it is operated in these SoC regions.

3 Model Application on Representative Cell Geometries

Now that the governing equations and assumptions are defined, in this chapter the implementation of the model into the solving software and its application for different representative cell geometries will be presented. At the beginning, a brief overview of the whole simulation process will be given in section 3.1. Then in section 3.2 the set-up of the cell geometry will be explained in detail and some examples will be shown. A model can only deliver reasonable results, when the modelling parameters have meaningful values. Some of them are calculated from experimental results, and the way how this is done will be sketched in section 3.3. An overview of all the calculated cases will be given in table form in section 3.4. The analysis and interpretation of the resulting data will then be presented in chapter 4.

3.1 Brief Overview of the Solving Mechanism

In this section an overview of the model solving procedure will be given. A more precise description of certain aspects can be found in the subsequent sections 3.2 - 3.4.

The model itself is implemented using the program **Elmer**, an *"open source multiphysical simulation software"* [49]. The software is based on the *finite element method*, a numerical method for solving sets of differential equations. The equations and specific settings are implemented in user defined *"Solvers"* which are based on the programming language Fortran. As an input, a so called *"Solver Input File" (SIF)* needs to be written which provides all necessary informations to **Elmer** in order to perform the calculations, e.g. the geometry used, the equations applied to the different parts of the geometry etc.

In order to perform a simulation with the finite elements method, a certain geometry consisting of such finite elements representing the cell, has to be created first and then given as an input for the solver software. Such a geometry is called *"Mesh"*. The software used to create these geometries is called **Salome** which *"provides a generic platform for Pre- and Post-Processing for numerical simulation"* [50]. The software is based on the programming language Python which allows to govern it with external Python scripts. The external script defines the geometry measures and other settings. The geometry is created automatically and the finished mesh is exported in the correct format, so it can be used by **Elmer**. All other scripts to govern the modelling process are written in Python as well.

The analysis of the Elmer results is done with **Paraview**; *"an open-source, multi-platform data analysis and visualization application"* [51]. It allows to look at the values of the independent model variables right at the geometry which enables a spatially resolved view on the occurring gradients. Another feature of the program is that the simulation progress can be viewed in real-time with the possibility to export the visualised data as a video.

Fig. 3.1 shows a small flow chart image of the software used and the order in which the specific programs are applied. As a first task the geometry has

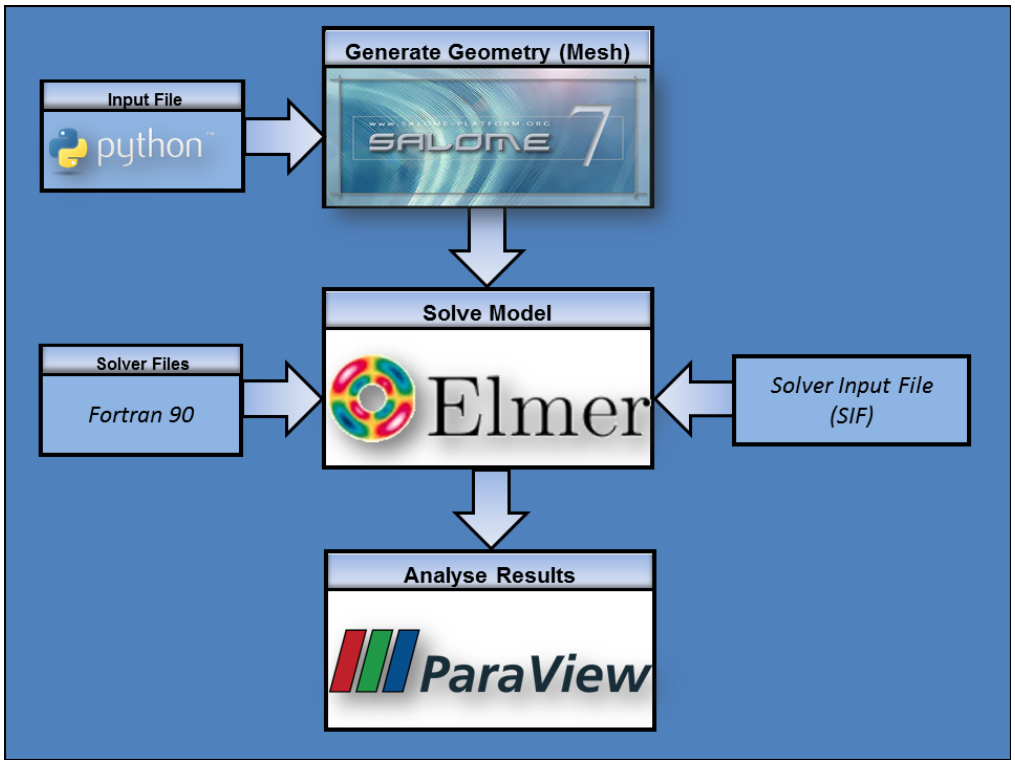

Figure 3.1: *Flow Chart depiction of the model solving process showing the dependencies of the different software used.*

to be created in order to perform a simulation. It is given as an input to **Elmer** which solves the governing equations in the finite elements of the mesh.

3.2 Explanation of the Testing Cell Geometry

In this section the set-up of the cell geometry which is used as an input for the Elmer solver is described in more detail and examples of created geometries are shown.

General Explanation The cell geometry used in the model consists of the three basic parts of a battery: anode, cathode and electrolyte/separator. In our model, the anode is considered to be a lithium metal electrode which does not change its form or composition during the simulation. Therefore, only its interface to the electrolyte is modelled and which is represented in the geometry as a simple plane which can absorb or release Li-ions into the electrolyte via an electrochemical reaction which is described in the model with a Butler-Volmer equation.

Adjacent to the anode plane is the separator regime. It basically consists of the electrolyte. In real batteries the separator is a porous medium, but in contrast to the cathode the exact geometry of the separator is not considered. Instead the *porosity* is a model parameter which influences the conductivity of the ions and the capacity of the separator, that is the number of ions that can be located therein. The range of the parameter is between 0 and 1. For example a porosity value of 0.6 means that the separator in the geometry consists of 60 % electrolyte and 40 % of the actual separator material. So the considered quantities will be reduced by a factor of 40 %. In the simulations the porosity of the separator was set to 0.5. In addition to the porosity, the *tortuosity* of the separator can be given. This parameter incorporates the longer way the ions have to go due to the separator geometry. It is in the same range as the porosity but only influences the ion conductivity and not the capacity.

From the geometrical point of view only a coarse mesh is used for the separator which means that it is only composed of a rather small number of finite elements. It is built up of planes parallel to the anode plane with a distance getting larger the farther away the planes are from the anode. The reason for this is that reactions, described by the Butler-Volmer equation, occur at the anode interface and Li ions enter (or leave) the separator. So the interface area is more interesting regarding gradients in the ion concentration than

the bulk electrolyte. Here, larger changes in these gradients are expected. The smaller distance between the planes at the interface incorporates these considerations.

Next to the separator is the cathode domain. It consists of electrolyte with a certain number of particles therein, arranged on a regular grid. The focus of the modelling effort is set on the cathode behaviour, so this region is viewed in more detail. Two different particle shapes have been considered, namely spherical and cubic particles. A more precise explanation of the advantages and disadvantages of the specific shapes is given in section 3.4. At the particle-electrolyte interface electrochemical reactions occur, when Li-ions enter or leave the particle. These lead to gradients in the ion concentrations in both domains. To get a better view at this particularly interesting region, some fine interface layers parallel to the surface of the particle have been introduced on the electrolyte side of the interface. In general it can be said that for the cathode bulk electrolyte a much finer mesh was used than for the separator and it thus consists of a much higher number of elements. Instead of parallel planes, the electrolyte space in the cathode is filled with triangular elements. The length of the cathode depends on the number of particles considered in the mesh. The more active material particles there are in the geometry, the longer the cathode has to be. The length of the separator in the model can be varied. A longer separator means a longer transport path of the Li-ions to travel from one electrode to the other which as a consequence, leads to larger gradients in the concentration.

Remarks on the Dimension of the Geometry With **Salome**, both 2D and 3D geometries can be created, and **Elmer** can treat them both without any problems. However, one has to consider which geometry is better suited for the problem. The three dimensional case is certainly more realistic since the geometry in real cells is three dimensional as well, and the information about

the behaviour of the model variables in all three space dimensions is relevant. But the main drawback when running the model on 3D geometries is the enormous computational effort. A 3D geometry consists of hundreds of thousands, up to more than a million finite elements. The biggest influence factor on the number of elements is how many active material particles there are in the cathode. So for a 3D geometry the number of particles is strictly limited. Exploiting the symmetry of the problem (explained in more detail below) can reduce the geometry size and allows to create geometries with some more particles, but it does not alter the fact that 3D geometries with a reasonable number of active material particles are nearly impossible to compute.

In Fig. 3.2a a 3D geometry is shown. In the image the specifications made above can be seen. At the right side there is the anode plane. The coarsely meshed area with the rectangular elements is the separator space. Adjacent to the separator there is the cathode, with has much smaller tetrahedral elements. The yellow elements are the active material particles. In this image the separator is of the same length as the cathode for a better representation in the image. For the simulations it was chosen to be twice as long as the cathode to achieve large gradients. The cathode of this example geometry consists of 81 particles in total, of which not all need to be represented in the mesh due to symmetry reasons. Larger geometries with up to 250 particles were possible to mesh, but the computation time, when applying the model to this geometry, was more than one day which was beyond any acceptable time scale. For this reason the geometry dimension has been reduced to 2D. The loss of one spatial dimension of course affects the way the geometry is built up and certainly has influence on the results. But simulations performed on 2D geometries showed reasonable results, so the influence of the geometry dimension was considered small enough to justify the use of 2D geometries for the purpose of this work.

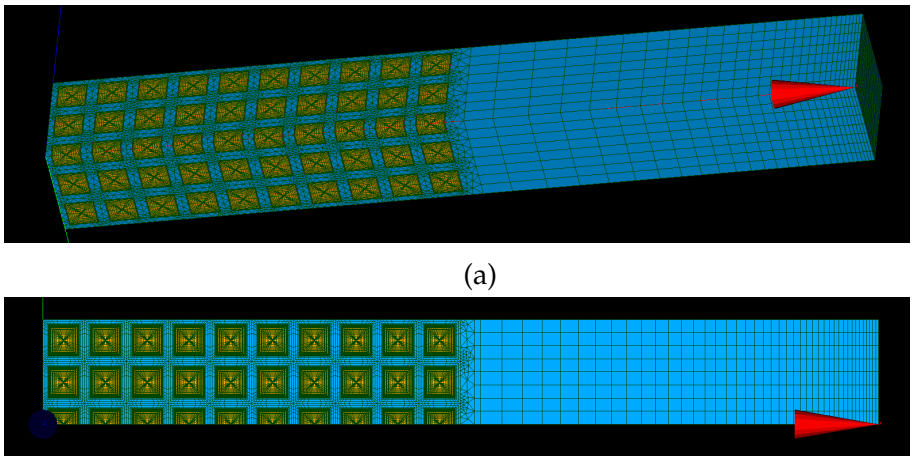

(a)

(b)

Figure 3.2: *Example of a 3D (**a.**)) and a 2D (**b.**)) geometry. At the right end is the anode plane, followed by the separator and the cathode with the active material particles in yellow. Due to symmetry reasons only a part of the whole geometry is represented in the mesh.*

The main advantage of the 2D geometries is that they consist of less finite elements and the calculations are thus much faster than for the 3D geometries. This gain in computation time can be used to create geometries with more particles in order to see, e.g. if a higher particle number has a significant influence on the results. Even with the larger geometries the computation time is still low enough to enable the calculation of a number of different cases in reasonable time.

Fig. 3.2b shows an example of a 2D geometry. The parts of the cell and their meaning is exactly the same as for the 3D case. At the right hand side there is the anode plane, followed by separator and cathode with the active material particles shown in yellow.

Exploiting the Symmetry of the Problem In the example geometries in Fig. 3.2, it has already been stated that not the whole cell geometry has to be meshed due to symmetry exploitation. How this is done, will be briefly

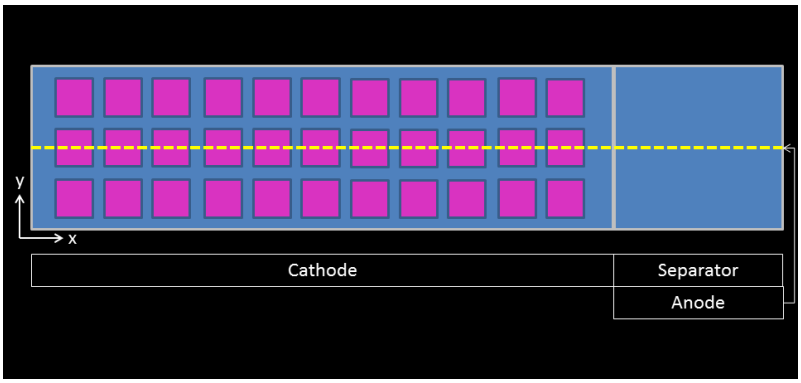

Figure 3.3: *Schematic drawing of a 2D cell geometry showing the full cathode with all particles. The particles are arranged on a regular grid. It is thus sufficient to mesh only the half of the geometry which is indicated by the yellow line.*

explained. Fig. 3.3 shows a schematic drawing of a 2D cell geometry with the full particle arrangement in the cathode. As can be seen, the particles in the cathode are arranged on a regular grid, so their centre points and the distances between the particles and their distances to the edges of the cathode are known. The separator and the anode, from a geometric point of view, are homogeneous areas consisting of only one material. As the yellow line in the figure indicates, it is sufficient to create only one half of the geometry in the y-direction. In the x-direction however the full length from anode to cathode is necessary to receive all the information.

For the 3D case the approach is completely analogous. The geometry is extended by one spatial dimension, so in total only one quarter of the full geometry has to be meshed.

As an example, a 3D cathode with 27 particles in total (3 particles in x y and z each) is considered. In the x-direction the geometry has the full length of 3 particles. In y- and z-direction only one and a half particles are created and meshed which gives a final number of $6\,^3/_4$ particles in the smallest repeatable unit.

3.3 Calculation of Modelling Parameters from Experimental Data

A series of experiments has been performed by an external project partner [52], with the goal to investigate NMC cathodes and electrolytes with different concentrations of Li-ions. Some of the experimental results have been used in order to calculate certain model parameters. When using a model to describe a physical process, it is of vital interest to have reasonable parameters. Otherwise the results might render unrealistic. Hence using experimental parameters in the model is expected to increase the validity of the results and, in further consequence, to give a better insight into the physical processes involved. For parameters with no experimental data available a value can be taken from the literature or it has to be fitted or simply estimated.

3.3.1 Mass Density of NMC

The cathode used in the electrochemical model consists of the layered TMO NMC. It is important to have some information on the crystal structure and also on the mass density of the material.

As already mentioned in section 2.5, this material has been widely investigated over the last decade. In this section the mass density of NMC will be calculated from its crystal unit cell and the values for the lattice parameters taken from Koyama et al. [30]. The atomic weights of the occurring elements have been taken from the book *"Das Basiswissen der Chemie"* by Mortimer [53]. The literature states a hexagonal crystal structure for NMC, as is shown in Fig. 3.4. The lattice parameters from Ref. 30 are used to calculate the

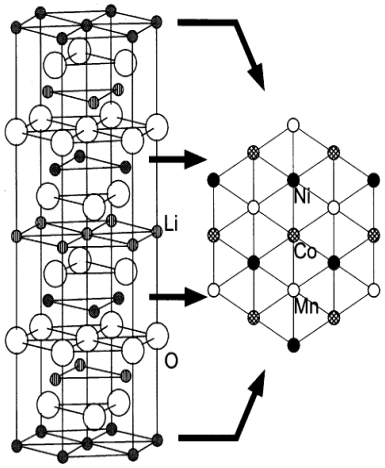

Figure 3.4: *Structural unit cell of NMC [30].*

Lattice Parameters [$\AA$]	Value
a	2.867
c	14.246
Atomic Masses [u]	Value
Ni	58.6934
Mn	54.9381
Co	58.9332
O	15.999
Li	6.94
Atoms in the unit cell	Value
NMC (ratio 1:1:1)	9
O	18
Li	9

Table 3.1: Crystal data used [30]

volume of the unit cell as a first step:

$$V_{UC} = \frac{3}{2} \cdot \sqrt{3} \cdot a^2 \cdot c = 304.229\,\AA^3 \tag{3.1}$$

From the volume of the cell, the density of the material can be calculated, if the masses of the involved atoms are known. The number of each type of atom in the cell can be obtained by counting. The mass of the atoms in the unit cell is now calculated by multiplying these numbers with the corresponding atomic weights:

$$m_{ges} = 3 \cdot m_{Ni} + 3 \cdot m_{Co} + 3 \cdot m_{Mn} + 18 \cdot m_O + 9 \cdot m_{Li} = 868.1361\,u \tag{3.2}$$

Finally, the density of NMC in atomic units is calculated by dividing the total mass by the volume of the unit cell:

$$\rho_{NMC,atom} = \frac{m_{ges}}{V_{UC}} = 2.8536\,\frac{u}{\AA^3} \tag{3.3}$$

The density is recalculated in terms of SI units:

$$\rho_{NMC,SI} = \rho_{NMC,atom} \left[\frac{u}{\mathring{A}^3}\right] \cdot \frac{1.660 \cdot 10^{-27}}{(1 \cdot 10^{-10})^3} \left[\frac{kg}{u}\right] \left[\frac{\mathring{A}^3}{m^3}\right] \tag{3.4}$$

$$\rho_{NMC,SI} = 4738.46 \, \frac{kg}{m^3} = 4.738 \, \frac{g}{cm^3} \tag{3.5}$$

The calculated value is of the order typical for a ceramic material and can thus be considered plausible.

3.3.2 Calculate Limits of the Lithium-Ion Concentration

In the model the concentration limits for Li-ions in the cathode have to be given as a parameter for a fully charged (concentration in the cathode is low) and a completely discharged (concentration in the cathode is high) cell. Due to reasons of structural stability, not all Li-ions can be extracted from the cathode during the charging process. The capacities of the cathode in full and empty state have been taken from measurements and are referred to as C_{min} and C_{max}. This data can be used ,together with the density of NMC $\rho_{NMC,SI}$ from above, in order to calculate these concentration limits c_{min} and c_{max}.

$$c_{max} \left[\frac{\text{mol}}{\text{m}^3}\right] = \frac{1}{F} \left[\frac{\text{mol}}{\text{As}}\right] \left(\rho_{NMC,SI} \left[\frac{\text{kg}}{\text{m}^3}\right] \cdot C_{max} \left[\frac{\text{As}}{\text{kg}}\right] \right) \tag{3.6}$$

$$c_{min} \left[\frac{\text{mol}}{\text{m}^3}\right] = \frac{1}{F} \left[\frac{\text{mol}}{\text{As}}\right] \left(\rho_{NMC,SI} \left[\frac{\text{kg}}{\text{m}^3}\right] \cdot C_{min} \left[\frac{\text{As}}{\text{kg}}\right] \right) \tag{3.7}$$

As an example the theoretical capacity of NMC is considered to be 278 mAh/g [29, 31] and is set as maximum value C_{max}. If for instance 50 % of the Li-ions could be extracted, the minimum capacity C_{min} would take the value 139 mAh/g.

For these values the approximate concentration limits would be:

$$c_{max} = 49150 \, \frac{\text{mol}}{\text{m}^3} \tag{3.8}$$

$$c_{min} = 24575 \, \frac{\text{mol}}{\text{m}^3} \tag{3.9}$$

3.3.3 Consider the Influence of Binder and Additives in the Cathode

In the geometry used for the simulations, the cathode consists active material particles which are embedded in electrolyte. In real cathodes, however, there is always a certain amount of conductivity additives and binder material to keep the particles together. In the model the assumption was that these materials are spread equally over the fraction of electrode space which was not covered by particles. To save computation time, additive and binder were not modelled separately, but instead, as it has already been done with the separator, they were considered by using a scaling factor for the conductivity and the capacity of the electrolyte.

The necessary data for calculating the fraction of additive and binder, were taken from experiments. Coin cells with a NMC cathode, a separator and a Li-metal anode were built by our partner in order to perform several charge and discharge experiments. The goal was to test the performance of the cathode in a real cell. The measures of the cathode of this cell were taken as a reference for the calculation. With the electrode thickness and diameter, its volume has been calculated. The mass fractions of the electrode have to be known and are given in percent, for instance 70 % NMC, 15 % of additive and 15 % of binder. The mass of NMC in the electrode was known, and so the masses of the other parts were obtained according to this mass ratio. In order to calculate the volume fractions of each material, the densities had to

be known as well. The density of NMC was taken from section 3.3.1 and the densities of additive and binder were taken from the literature. For the density of a species, the following formula was taken:

$$\rho_i = \frac{m_i}{V_i} = \frac{m_i}{p_i \cdot V_{electrode}} \tag{3.10}$$

In the equation ρ_i is the density, m_i, the mass, V_i the volume and p_i the fraction of the specific species i of the electrode volume. $V_{electrode}$ is the volume of the electrode. Solving the equation for p_i yields:

$$p_i = \frac{m_i}{\rho_i \cdot V_{electrode}} \tag{3.11}$$

With this formula, the volume fractions of NMC, additive and binder were obtained. All three volume fractions, together with the electrolyte filling the electrode pores, must result in the total electrode volume. So the electrolyte fraction is known as well.

In the model geometry, the particles are assumed to consist of pure NMC. So the additive and the binder, together with the actual electrolyte, share the "electrolyte" volume in the geometry. To get the fractions of the specific species in this volume, their fraction of the total electrode were divided by the sum of the three species.

The calculations yield that the fraction of the cathode, not covered by active material particles, consists of about 80 $\%_{Vol}$ electrolyte and 20 $\%_{Vol}$ additive plus binder. The conductivity and the capacity of this phase in the model were scaled according to this result. The actual fraction of electrolyte in the "electrolyte" space of the cathode in the further course will be referred to as cathode porosity p_C.

It needs to be pointed out that this calculation can only be an estimation of the real volume fractions in the electrode. During the manufacturing

process all ingredients of the electrode are mixed together in a powder and compressed under high pressure. It is not clear, how the densities of the specific materials change during compression, since the compressibility of the species is unknown as well as the exact manufacturing conditions.

3.3.4 Approximation of the Open Circuit Voltage from Pulse Test Data

As already mentioned, real coin cells were set up in order to perform a series of cycling tests which consist of a specific sequence of cell charging and discharging events in order to obtain information about the cathode behaviour in a real cell. Part of these tests were short charge or discharge pulses with a specific current at different SoC values of the cell. This measurement data was used to get more realistic values for several model parameters. One of them is the OCV, that is the cell voltage without load which corresponds to an electrochemical equilibrium state of the cell. It is an SoC dependent quantity. After the short pulses there is always a relaxation time, where the cell goes back into equilibrium which means that the cell voltage will relax to its OCV value after a certain period of time. The voltage values after the relaxation period were taken from these pulses with different SoC values and a polynomial curve was fitted to these data points in order to obtain an approximation of the OCV over the whole SoC range of the cell. The shape of such an OCV has already been shown in Fig. 2.7. Of course one has to take care when doing such an approximation that the relaxation time is chosen long enough, so that all gradients are relieved. Otherwise, the obtained values are not correct and do not represent the equilibrium cell voltage.

3.4 Model Testing for Different Representative Cases

3.4.1 Remarks on the Particle Shape

In order to perform the simulations, two different particle shapes have been considered, namely spherical and cubic particles. In this section the advantages and disadvantages of both shapes are briefly discussed.

The advantage of spherical particles is certainly that they would be the more realistic case. There are some drawbacks with this shape, however. The first thing is that creating mesh geometries with spheres is computationally very expensive. All the geometric forms in the mesh consist of finite elements and if one wants to have "round" spheres a very high number of elements is needed to realise this. When the spheres itself have a high number of elements, the surrounding electrolyte needs a fine element resolution as well. As an example a rather small 3D geometry of 125 particles is considered, whereof 31 1/4 (one quarter due to symmetry, see section 3.2) actually have to be meshed. With spherical particles the mesh consists of more than 750 000 elements (edge, surface and volume elements) which is already a high number. Bigger geometries would consist of millions of elements which drastically increases the computation time and makes reasonable calculations virtually impossible.

Another disadvantage arising from the use of a particle with a spherical shape is the low packing density when the particles are arranged on a regular grid (the simple cubic crystal system has a packing density of $\sim$ 52 %). So, there will always be a significant amount of electrolyte in the cathode, even though the distance between the particles is made very small.

All these reasons lead to the switch to cubic particles. Their disadvantage is that they do not depict the real situation as good as spherical particles, but on the other side, they excel in terms of operability. The cubes are meshed faster than the spheres and the geometries consist of less finite elements. For instance the same 3D geometry with 125 particles consists of about 500 000 elements which is a number reduced by about one third compared to spherical particles and reduces of course the computation time. The number of elements in the particle and their distribution across it can be set easily as well as the interface layers on the electrolyte side. Another disadvantage using spherical particles, can be circumvented. Cubic particles can be brought closer together, so distributions with small distances between the particles are possible. So for testing cases with small particle distances, a cubic shape is thus considered to be the more suitable solution. Due to the reduction in the mesh elements, bigger geometries can be realized.

A direct comparison of a spherical and a cubic particle can be seen in Fig. 3.5. An example of a spherical particle is shown in Fig. 3.5*a*. The yellow area is the actual particle and the magenta coloured area represents the interface layers which actually belong to the electrolyte domain and were introduced in order to better handle the gradients. The electrolyte domain itself is the blue area. Fig. 3.5*b* shows an example of a cubic particle. Again the actual particle is yellow and the interface layers are shown in magenta. If the two shapes are compared, the points discussed above are obvious. The spherical particle consists of much more elements than the cubic particle which drastically increases the computational effort, when geometries with many particles are involved. All these considerations are only partially valid for the 2D case, since the term “particle” has a slightly different meaning there. In x- and y-direction there is the same situation as for the 3D case. In the z-direction, however, there are no separated particles but long cuboids or cylinders dependent on the particle shape.

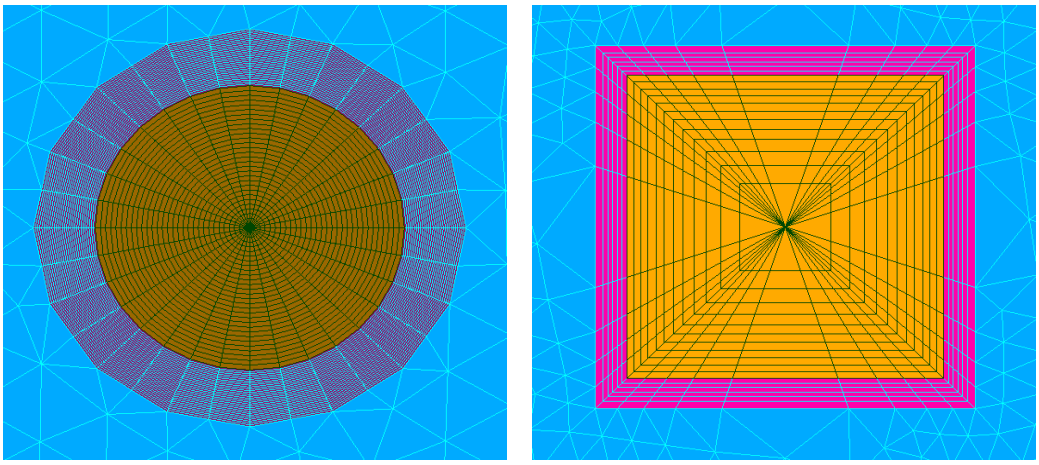

(a) (b)

Figure 3.5: *Direct comparison between a spherical **(a)** and a cubic particle **(b)**. In both images the actual particles are shown in yellow. The magenta area represents the interface layers. The surrounding electrolyte domain is shown in blue.*

3.4.2 Current Profiles as Input for the Model

When running a simulation, a certain sequence of charging, discharging or relaxation events has to be given as an input for the model solving framework. This sequence will be referred to as *profile* over the further course of the thesis. For charging and discharging events, a current and a time span have to be given as input parameters. When simulating a relaxation phase, the current is set to zero. A discharge current in the model has a positive value, a charge current a negative one. In the simulations, the response of the cell to such an input current is calculated, regarding concentration and potential gradients across the geometry, as well as the cell voltage.

In order to avoid unnecessary complexity and to keep computation times in a reasonable order of magnitude, a relatively simple profile has been chosen. For most cases a single discharge pulse with a length of 100 s and a current

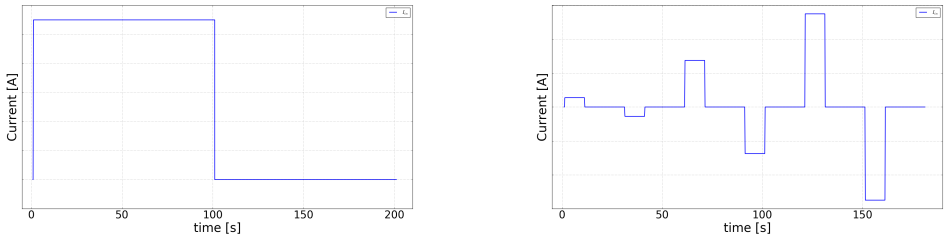

(a) (b)

Figure 3.6: ***(a)*** *Input current for a single discharge pulse, followed by a* 100 *s relaxation time.* ***(b)*** *Input current for a sequence of three discharge/charge pulses, each* 10 *s long, with a relaxation time of* 20 *s in between.*

of 5 C has been defined. The pulse was followed by a 100 s relaxation time with zero current, where the cell goes back into electrochemical equilibrium and the gradients are reduced. In Fig. 3.6*a* the shape of the input current can be seen for a single discharge pulse.

Another profile that has been used was a sequence of three discharge/charge pulses with different currents (an example for such a pulse can be seen in Fig. 3.6*b*). In the example each pulse is 10 s long, followed by 20 s of relaxation. The C-rates of the pulses were chosen to be 0.5, 2.5 and 5 C. The actual current is calculated from these C-rates by using the cell capacity.

3.4.3 Plausibility Analysis of the Model and its Sensitivity to Parameter Variation

When a new model is set up, it is always important to test if the results of the performed calculations are plausible and do not reveal any contradictions to physical principles or validated experimental results. If the model has passed those tests and it can be seen as reliable, and it can be used to gather

information about issues that are not directly accessible by experiment and can lead to new insight to the involved physical processes.

Another important issue is the sensitivity of the model to a variation in the model parameters. The question is, how does the model react if a parameter is changed and when do instabilities occur in the numerical simulations.

A part of this thesis was such a plausibility and sensitivity analysis of the model. Several model parameters have been chosen and have been varied from very low to very high values in order to reveal their effect on the results. In order to test the influence of each parameter alone, as a first part, only one parameter was changed in a test series, and the others were kept at constant values. To find out if there are cross effects between the parameters and the how the change of one parameter can influence the others, in the further course several parameters were changed at once. All the calculations for these test series were done on 2D geometries.

The parameters chosen for this kind of analysis were the solid state diffusion coefficient D_0, the reaction constant on the cathode side k_{BV}, the cathode porosity p_C, the initial state of charge (SoC) of the cell and the charge or discharge current (C-rate). An overview of which test series have been performed is given in section 3.4.5 and the results are presented in chapter 4.

3.4.4 Testing the Influence of the Pore Size Distribution on the Cell Behaviour

Contrary to previous models from the literature, in the electrochemical battery model used in this thesis two different pore sizes for the particles in the cathode can be given. One aim of this thesis is the testing of the influence of those different pore sizes in the cathode on the performance of the cell.

Does the particle arrangement in the cathode and thus the distribution of the pores affect the cell behaviour, and if it does, how big is the influence and how can it be controlled? In order to tackle such a goal, test geometries as described in section 3.2 have been created and then the model has been applied to these geometries.

A model testing procedure was established. For each test series geometries with two different pore size distributions have been created. A test series is defined by the following specific parameters:

1. Number of particles in the cathode
2. Size and shape of the particles
3. Measures of cathode and separator
4. Fixed setting of the model parameters (e.g. diffusion coefficient)
5. Other details concerning the geometry, for instance the fineness of the mesh, etc...

The first case to take a look at in each test series was a cathode with equally distributed particles. The distance between the particles was the same in all considered space directions. The other extreme case were aggregates, comprising a certain number of particles with extremely small distances between the particles inside the aggregate and large distances between the aggregates. Between these two extreme cases several geometries with an intermediate distance between the particles in an aggregate can be created as well, in order to investigate if there is a continuous change in behaviour depending on the minimum pore size. To assure that potential differences in the behaviour really result from the difference in the particle arrangement, it was explicitly minded that particle number and size did not change throughout a testing series. In other words, the porosity of the cathode, namely the volume share covered by electrolyte, has been kept constant as well as all the other adjustable model parameters.

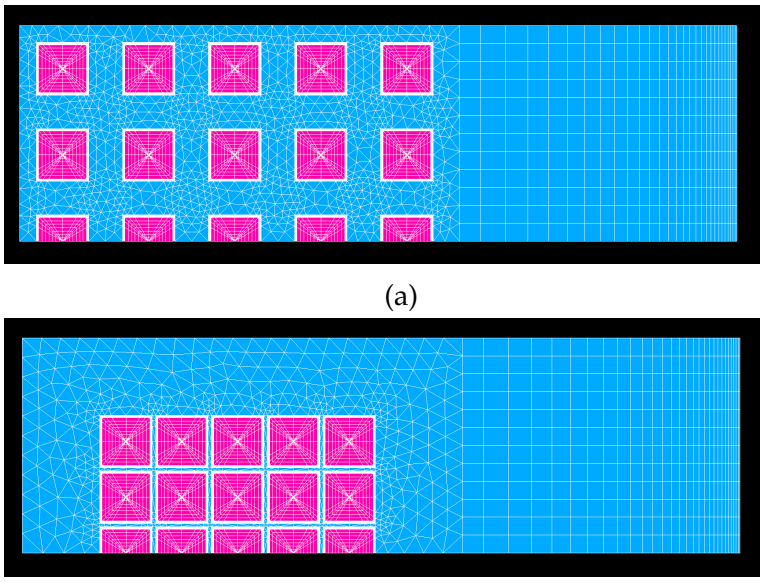

(a)

(b)

Figure 3.7: **a.)** Geometry with particles distributed equally over the cathode space. **b.)** Geometry with particles compressed to an aggregate with small distances inside the aggregate and a large electrolyte space outside.

A small example geometry, one with equally distributed particles, one with aggregated particles is shown in Fig. 3.7. In the geometry file the grade of aggregation is defined by stating the ratio between small and big pores. A ratio of 1.0 means equally distributed particles, since the small and the big pores are of the same size. A value of 0.1 would mean that the big pores are ten times as big as the small pores. For most of the calculations a ratio of 0.02 was used for the aggregated case, so there is a factor of 50 between the two pore sizes. Values smaller than 0.02 could not be realised due to the limits of the discretisation of the mesh. When the size of a cathode geometry is given, this is done in terms of the size and the number of these aggregates. The size of an aggregate is defined by the number of particles in x-direction. For instance, the geometries in Fig. 3.7 consist of one aggregate with five particles in each direction and a total number of 125 particles.

3.4.5 Overview of Performed Test Series

All considerations regarding geometry dimension and particle shape led to the decision to perform all test series with 2D geometries and cubic particles. The size of the geometry was chosen to be a mesh consisting of three aggregates with a length of seven particles. The cathode was 30 µm long, the separator had a length of 60 µm. The particles had a side length of 1 µm. All test series have been performed for room temperature (= 303 K) and an anode reaction constant of $k_{Li} = 10^{-3}$ which scales the reaction kinetics at the interface between anode and the electrolyte.

Here, a short overview of all the performed simulations and their settings will be given in table form. The detailed results of all performed test series along with their physical interpretation will be given in chapter 4. All parameters relevant for the calculation will be given in the table in order to have the most important settings at a glance.

Explanation of the Table The test series information can be found in Tab. 3.2. The first column *Name* gives a short description of the series with its main goal. The column *Section* describes, in which section the results can be found. *Prof* defines which current input profile has been used with the corresponding C-rate(s) in *C*, *SP* as profile name stands for a single discharge pulse, *TP* for three discharge pulses with different C-rates. The columns D_0, k_{BV}, p_C and *SoC* list the parameter values for the OOM for the particle diffusion coefficient, the reaction constant on the cathode side, the cathode porosity and the initial state of charge respectively. If the parameter was varied in the specific test series the minimum and maximum values are given.

Table 3.2: Overview on performed test series. For the meaning of the abbreviations see bottom of the table.

Name	Section	Prof	C	D_0	k_{BV}	p_C [%]	SoC [%]
D_0 Variation	4.1.1	SP	5	10^{-5}-10^{-15}	10^{-3}	80	50
k_{BV} Variation	4.1.2	SP	5	10^{-10}	10^{+1}-10^{-11}	80	50
p_C Variation	4.1.3	SP	5	10^{-10}	10^{-3}	5 - 100	50
SoC Variation	4.1.4	SP	5	10^{-10}	10^{-3}	80	20-100
Cross Effects 1	4.2.1	SP	5	10^{-10}-10^{-15}	10^{-3}	80	20 - 100
Cross Effects 2	4.2.2	SP	5	10^{-10}	10^{-3}	10-50	20 - 100
Triple Pulses	4.2.3	TP	0.5, 2.5, 5	10^{-10}-10^{-15}	10^{-3}	80	20,50,100

Abbreviations: *Prof ... Current Profile, SP ... Single Pulse, TP ... Triple Pulse, C ... C-Rate, D_0 ... OOM of the particle diffusion coefficient, k_{BV} ... cathode reaction constant, p_C ... cathode porosity, SoC ... state of charge*

4 Results and Discussion

In this chapter the results of the model calculations are presented and analysed. As mentioned in section 3.1 data visualization was done with the program **Paraview**.

The chapter is separated into four sections. At first model parameters are varied in order to test their influence on the cell behaviour. In section 4.1 each of the selected parameters is varied individually in order to investigate its isolated impact on the results. This is followed by test series, where more than one parameter has been varied in order to check the results for possible cross effects. These results can be seen in section 4.2. In this section also the simulations with different C-rates are shown.

How the particle arrangement in the cathode influences the cell behaviour is an important question of this thesis. Therefore, all the simulations presented here have been done twice; once for equally distributed particles in the cathode and once for particle aggregates. In section 4.3 it will be discussed, how the performed parameter variations affect the influence of the geometry used and for which values of the parameters the geometric arrangement becomes important and in which parameter regimes it is negligible.

In Tabs. 4.1 and 4.2 the specifications regarding the geometry and the two different current input profiles for the simulations are given. The current profiles were described in more detail in section 3.4.2. All the simulations

were performed on a 2D geometry consisting of three particle aggregates with a length of seven particles each. For each of the test series, at the beginning the parameter ranges are given in form of a short table.

Parameter	Value
Aggregate size	7
Aggregate number	3
Pulse time	100 s
Relaxation time	100 s
C-rate	5

Table 4.1: Specifications for the single pulse current profile

Parameter	Value
Aggregate size	7
Aggregate number	3
Pulse time	10 s
Relaxation time	20 s
C-rate	0.5, 2.5, 5.

Table 4.2: Specifications for the triple pulse current profile

4.1 Plausibility and Sensitivity Analysis - Variation of Model Parameters

The governing equations require knowledge about a number of parameters, in order for the model to provide reasonable results. The best way to determine the value of such a parameter, is to measure it in an experiment, which has been done by our partner for several parameters. The problem is that not all parameters, such as the reaction constants in cathode (k_{BV}) and anode (k_{Li}) or the OOM of the diffusion coefficient in the cathode particles (D_0), are directly measurable. To get a better feeling of how these parameters influence the behaviour of the cell and of how sensibly the model reacts to changes of their values, the simulation was run several times with different OOM of a specific parameter. In other words, the parameter of interest was set from very small to very large values in a certain number of steps and the results were compared. This has also been done for the cathode porosity p_C, although for this parameter measurement data is available and has been

implemented in the model (see section 3.3.3). It has been varied nevertheless, because of its major influence on ion transport in the electrolyte. Another parameter that has been varied, was the initial state of charge *SoC* of the cell. For the *SoC* no *"correct"* or *"realistic"* value needs to be found, but a fully charged cell behaves obviously different than a discharged one.

The results are shown below. In this section each of the selected parameters is varied individually. The varied parameters are

- the scaling factor of the diffusion coefficient D_0
- the cathode reaction constant k_{BV}
- the cathode porosity p_C
- the initial state of charge *SoC*

The anode reaction constant k_{Li} has not been chosen for variation, since the anode is not modelled in detail and a change in the reaction rate would simply tune the resistance for the ions to get transferred from the anode into the separator, without changing the basic behaviour of the cell.

4.1.1 Variation of the Particle Diffusion Coefficient D_0

In Tab. 4.3 the parameter specifications for the test series are shown. Geometry and current profile used are described in Tab. 4.1. The diffusion equation for the cathode particles is shown as a reminder.

Parameter	Value
$\boldsymbol{D_0}$	$\mathbf{10^{-5}}$ **-** $\mathbf{10^{-15}}$
k_{BV}	10^{-3}
p_C	80 %
SoC	50 %

Table 4.3: Specifications of the D_0 test series

$$\frac{\partial c_s}{\partial t} - \nabla \cdot (D_s \nabla c_s)) = 0 \tag{4.1}$$

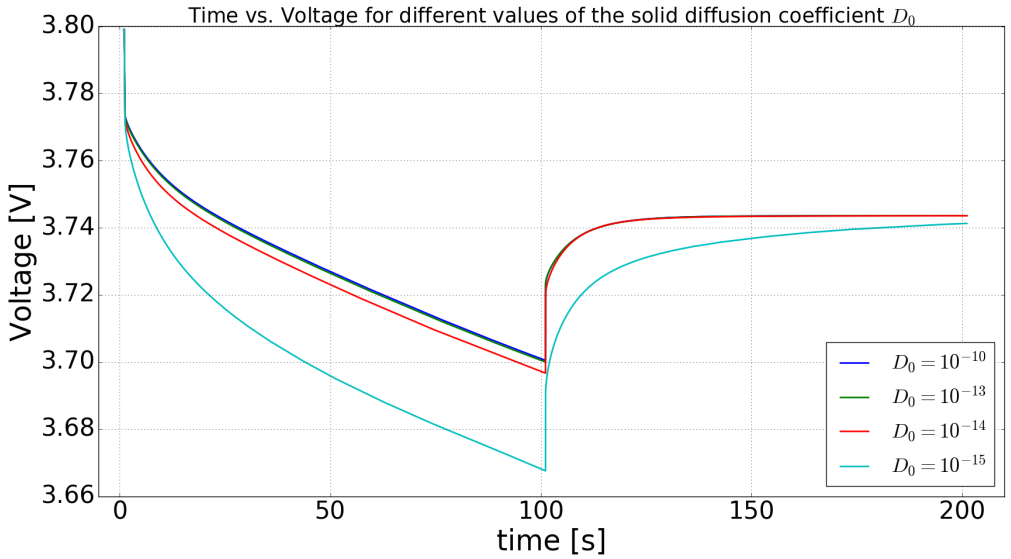

Figure 4.1: *Cell voltage for different values of the solid diffusion coefficient* D_0*. The results for* $D_0 = 10^{-10}$ *and* 10^{-13} *are almost the same. Significant differences occur for values below* $D_0 = 10^{-13}$

After a Li-ion has entered a particle in the cathode, the following transport inside the particle is described by diffusion. The parameter which determines the velocity of this process is D_s. As already mentioned in section 2.7, it is written as a product $D_s = D_0 \cdot D_s^*(SoC)$ of an SoC dependent part D_s^* with the unit $\mathrm{m^2\,s^{-1}}$ and a scaling factor D_0 which defines the OOM of the diffusion coefficient. For a better readability this scaling factor will be referred to as diffusion coefficient in the further course of the thesis. To investigate, how a very fast or a very slow diffusion process would change the cell behaviour, D_0 has been varied from a very high value of 10^{-5} to a very low value of 10^{-15}. The calculations were performed at 50 % initial SoC, with a cathode reaction constant $k_{BV} = 10^{-3}$ and 80 % cathode porosity.

In Fig. 4.1 the results of the simulation for the calculated profile can be seen. For relatively high values of D_0 (10^{-10} and 10^{-13}), the behaviour of the cell voltage is nearly the same, so the curves are almost undistinguishable. When

D_0 is high, it is not the limiting factor in the simulations and small changes do not have a big influence on the results. So running the simulation with even higher values did not give new informations which is why these curves are not shown in the figure. When the OOM of D_0 decreases, changes in the shape of the curve can be seen. The voltage drop over the course of the pulse gets larger. A significant difference can be seen between the values $D_0 = 10^{-14}$ and $D_0 = 10^{-15}$. Lower values have been tested as well and showed an even larger voltage drop, but then also numerical instabilities occurred during the simulations.

The voltage answer to the input current profile is calculated in the simulations. A discharge current causes the voltage to drop and to take a lower value than for the electrochemical equilibrium. This voltage drop consists of two basic parts. There is an initial voltage drop which occurs immediately after the current is switched on, and an additional voltage drop which evolves over the course of the discharge pulse.

In the figure it can be seen that the initial voltage drop does not seem to depend on D_0 at all, since it is exactly the same for $D_0 = 10^{-10}$ and $D_0 = 10^{-15}$. So the reason for this initial drop is not the diffusion in the solid particles, but has to be a different physical effect. It is assumed at this point that the electrochemical reaction at the interface between electrolyte and particle as well as the contribution from the electrolyte resistance, are the limiting factors at this stage and thus determine the magnitude of this initial voltage drop. In section 4.1.2 the reaction constant on the cathode side k_{BV} will be varied in order to test how different OOM of that parameter affect the cell behaviour.

After that initial voltage drop, the value of the diffusion coefficient well affects the further behaviour, regarding the shape of the curve and the total voltage drop throughout the full discharge pulse. In these simulations

the reaction constant was set to a relatively high value, so the transfer of Li-ions from the electrolyte into the particle was not the limiting factor. A small D_0 value means that the ions in the solid particles diffuse from the surface of a particle to its centre only very slowly, and a large concentration gradient inside a particle gets established; the Li-ions accumulate at the particle surface; whereas their concentration in the centres is much lower. For the charge transfer, only the concentration at the surface is relevant. When it is high, the particles locally have a different *SoC* and thus have a different OCV value, than they would have for a fast diffusion. Since the particles have a higher ion concentration, the *SoC* is lower and therefore also the voltage is lower. To keep the current up, a higher overpotential gets established which causes the higher voltage drop for the low diffusion case.

A segment of the cathode geometry for equally distributed particles can be seen in Fig. 4.2*a*. It depicts a case with a very slow solid state diffusion. The image was recorded for $D_0 = 10^{-15}$, a few seconds after the current has been switched on. In the image the red colour indicates a high values of the Li-ion concentration, and the blue colour means a low value. The smooth blue area is the electrolyte. Its behaviour is as expected. There is a gradient in the Li-ion concentration from the right to the left (from anode to cathode). It is very similar to the result of simulations with higher D_0 values. The behaviour in the cubic particles however, strongly differs from fast diffusion cases. The gradients of the Li-ion concentration inside the particles are very large and become even larger, when the discharge of the cell progresses. The ions get stuck at the particle surface, because they cannot diffuse away in time.

In Fig. 4.2*b* a cross section of the concentration through the centres of the particles has been made along the x-axis. It shows the situation at the beginning of the discharge pulse. The magnitude of the concentration

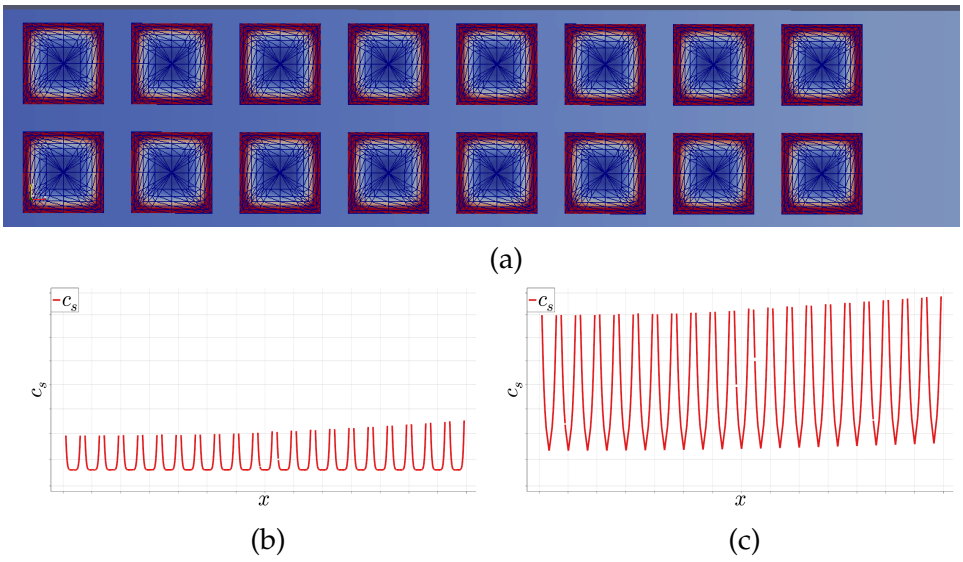

Figure 4.2: ***a.)*** *Segment of the cathode for a simulation with* $D_0 = 10^{-15}$. *The image was recorded a few seconds after switching on the current.* ***b.)*** *Line plot across the x-axis of the cathode, cutting through the particle centres, showing the Li ion concentration* c_s. *The slow diffusion causes large gradients inside the particles.* ***c.)*** *Same plot as for b.) after the full* 100 *s of the discharge pulse. Note the higher ion concentration in the particles.*

gradients can be seen. The particles at the right hand side are nearer to the anode and thus have a higher concentration at the particle edges, because the ions arrived there first. The concentration in the particle centres is the same for all particles which indicates that a few seconds after switching the current on, the ions which were transferred into the particles, did not reach the particle centre yet. Over the further course of the discharge pulse, the ions eventually will reach the particle centres and an overall concentration gradient in the particles along the x-axis will get established, as it can be observed for the high diffusion case. The Li-ion concentrations in the particles after the full discharge pulse is shown in Fig. 4.2*c*. It can be seen that the concentration is also higher in general due to the new, lower *SoC*.

When the current has been switched off, the system relaxes into an equilib-

rium state and the cell voltage goes back to the OCV value, dependent on the actual *SoC* of the cell. The established gradients in the Li-ion concentration, both in the particles and in the electrolyte, start to diminish. This happens by diffusion, again both in the particles and the electrolyte, and by charge transfer reactions from the particles back into the electrolyte. When looking at Fig. 4.1, right after switching the current off, there is again an immediate voltage change, now in the reverse direction which may be assigned to the contribution of the BVE in the model and the resistance of the electrolyte. This is nearly the same for all values of D_0. The subsequent part is different for low and high diffusion cases. In contrary to all other values, the cell voltage for $D_0 = 10^{-15}$ has not reached its equilibrium value after 100 s. This can be explained by taking a look at the different gradients that are present in the cell. At first, there is the gradient in the Li-ion concentration in the electrolyte reaching from anode to cathode. When looking at the results in **Paraview**, this gradient is relieved rather fast and is thus not assumed to cause the slower relaxation for $D_0 = 10^{-15}$. There are also gradients in the particles. On the one hand there are concentration differences between the particles and on the other hand there are gradients inside the particles. Analysis of the simulation results leads to the conclusion that the limiting factor in the relaxation are the gradients inside the particles which for $D_0 = 10^{-15}$ are still present after the 100 s of relaxation, whereas the gradients between the particles were already relieved. This can be seen in Fig. 4.3. There are no gradients between the particles any more, but still significant gradients

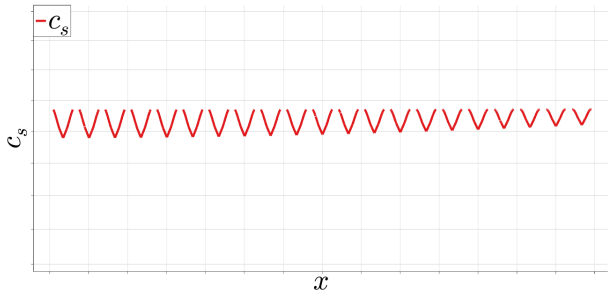

Figure 4.3: *Concentration in the particles across the x-axis of the cathode geometry at the end of the relaxation period.*

inside the particles. In general it can be said that the charge transfer reactions during relaxation are low compared to the case with a flowing current, because there are only very low overpotentials of a few mV present, due to the concentration differences between the particles. As a conclusion it can be stated that a slow diffusion has a significant negative influence on the cell behaviour during the discharge and the relaxation period.

Even those values for D_0 referenced to as small in this section are still quite large compared to self or foreign-atom diffusion in metals or alloys. The reason for this discrepancy is that the particles in the model are not single crystal and the diffusion is not due to atomic hopping only. The particles are assumed to be agglomerates of smaller crystals with grain boundaries and empty spaces in between which serve as high diffusivity paths. The D_0 value here is an average value over the particle agglomerates.

4.1.2 Variation of the Cathode Reaction Constant k_{BV}

In Tab. 4.4 the parameter specifications for the test series are shown. Geometry and current profile used are described in Tab. 4.1. Below the BVE describing charge transfer across the interface particles/electrolyte, is shown as a reminder.

Parameter	Value
D_0	10^{-10}
$\boldsymbol{k_{BV}}$	$\mathbf{10^{+1}\text{-}10^{-11}}$
p_C	80 %
SoC	50 %

Table 4.4: Specifications of the k_{BV} test series

$$j_{BV} = i_0 \cdot \left(\frac{c_l}{c_{l0}} exp\left(-\frac{\alpha F}{RT}\eta\right) - exp\left(\frac{(1-\alpha)F}{RT}\eta\right)\right) \tag{4.2}$$

At the interface between the active material particles and the electrolyte in the cathode, chemical reactions occur, where the Li-ions get reduced

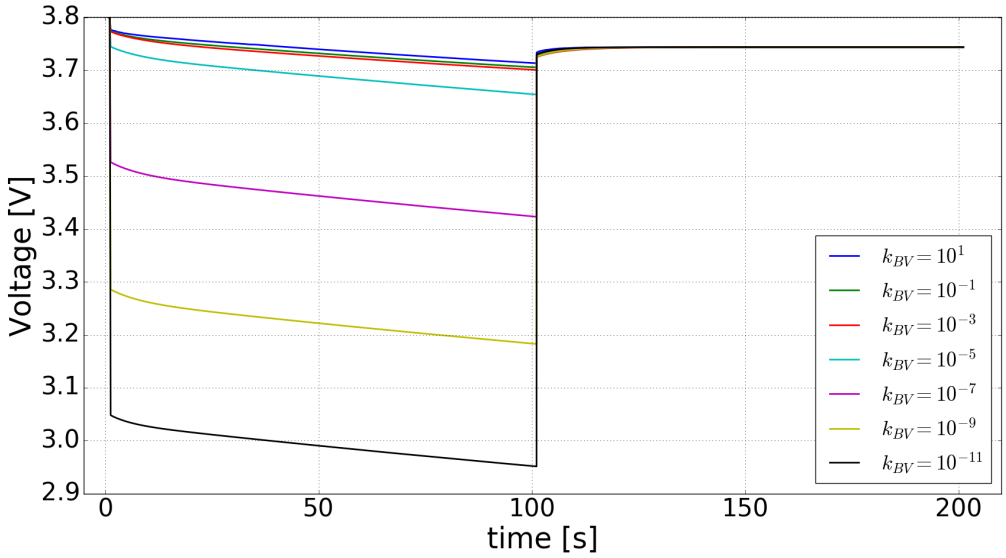

Figure 4.4: *Cell voltage for different values of the cathode reaction constant k_{BV}. Values of $k_{BV} \geq 10^{-3}$ show very similar results. For lower values the initial voltage drop increases significantly.*

or oxidised and enter or leave the particle. As specified in section 2.7, the exchange current can be written as a product $i_0 = k_{BV} \cdot i_0^*(SoC)$. The reaction constant k_{BV} influences the OOM of i_0, whereas the actual value i_0^* with the unit $\mathrm{A\,m^{-2}}$ depends on the SoC. This quantity describes the net current density in the BVE in dynamic equilibrium without any current. The higher it is, the more ions surpass the barrier. When a current gets applied, this equilibrium gets disturbed, and either the forward or the backward reaction gets enhanced. The simulations were performed for different OOM of k_{BV}, at a medium SoC of 50 % and a relatively high diffusion constant $D_0 = 10^{-10}$, to make sure that diffusion will not be the limiting factor in the simulations. The cathode porosity was set to 80 %.

In Fig. 4.4 it can be seen that the variation of this parameter heavily affects the voltage drop right after switching the current on and the voltage increase after switching it off again. The reason for this is that, as mentioned above,

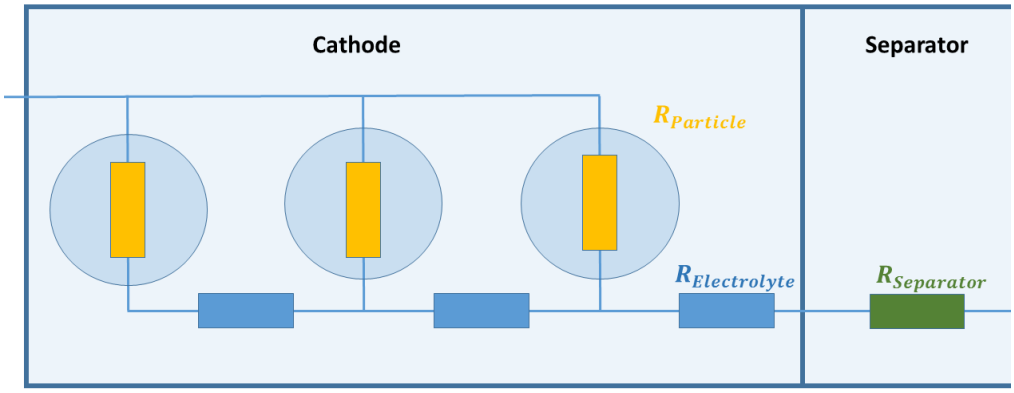

Figure 4.5: *Equivalent circuit diagram for the cathode and the separator of the cell. Every particle acts like an electrical resistance and so does the electrolyte in between the particles and in the separator.*

k_{BV} determines the OOM of the exchange current density i_0. A low value impedes the charge transfer process and less ions can surpass the energy barrier at the interface between particle and electrolyte. This leads to a high charge transfer resistance and thus to a high initial voltage drop. The magnitude of this voltage drop reaches from less than 0.1 V at values of $k_{BV} > 10^{-5}$ to more than 0.7 V for $k_{BV} = 10^{-11}$. When the current is switched off again, this resistance disappears and a corresponding relaxation can be seen. The additional voltage drop during the pulse seems not to depend strongly on the value of k_{BV}, but more on D_0, as seen in section 4.1.1, or other effects. How a low charge transfer current density impacts the cell behaviour can be explained with a simple equivalent circuit diagram for a part of the cell which is shown in Fig. 4.5. The wires show the possible pathways for Li-ions. The squares represent resistances which occur in the electrolyte and in the particles. Every ion has to pass the separator which corresponds to the green resistance $R_{separator}$. In the cathode, the electrolyte can be seen as number of resistances (blue) as well. The better the conductivity of the electrolyte, the smaller are these resistances. An ion has to enter a particle in order for a current to flow, and these transfer is

represented as a resistance too, shown in yellow in the figure. The resistance in the particles is mainly determined by the charge transfer which is scaled with k_{BV}. So if the reaction constant is small there is a higher resistance in the particles than there is in the electrolyte. The ions will choose the way with the lowest total resistance. Since the electrolyte resistance is considered to be low in this case, the ions will split up over all the particles equally and the charge transfer into the particles is the limiting factor which is mainly assigned to be responsible for the initial voltage drop when switching a current on. So a decrease in k_{BV} significantly increases this voltage drop. For the high values of k_{BV} in Fig. 4.4, namely $k_{BV} \geq 10^{-3}$, the initial voltage drop is low and very similar for the higher k_{BV} values. In this regime the charge transfer resistance across the interface is considered to be that low that a further increase of the parameter does not change the results any more. There is still a low but noticeable initial voltage drop which results from the contribution of the electrolyte resistance. For low k_{BV} values however, the voltage drop seems to be directly proportional to the value of k_{BV}, since the differences between the curves for $k_{BV} \leq 10^{-5}$ are approximately 0.12 V of additional voltage drop per order of magnitude. This can be seen in Fig. 4.6 which shows the total voltage drop caused by the discharge current versus the corresponding k_{BV} values. After k_{BV} undercuts a certain value, there is an exponential increase in the voltage drop with decreasing k_{BV} which corresponds to a linear increase with the OOM of k_{BV}

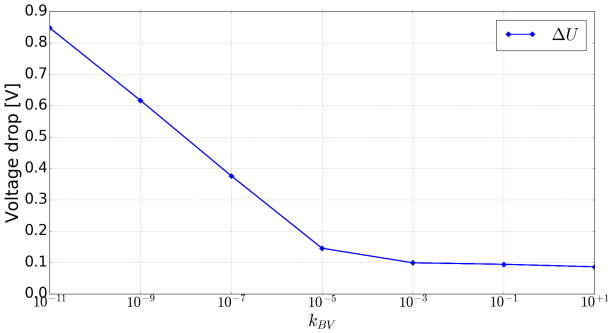

Figure 4.6: *Comparison of the total voltage drop for simulations with different k_{BV} values.*

4.1.3 Variation of the Cathode Porosity p_C

In Tab. 4.5 the parameter specifications for the test series are shown. Geometry and current profile used are described in Tab. 4.1. The cathode porosity p_C in % scales the electrolyte conductivity κ and capacity.

Parameter	Value
D_0	10^{-10}
k_{BV}	10^{-3}
pC	**5 - 100 %**
SoC	50 %

Table 4.5: Specification for the p_C test series

$$p_C \frac{\partial c_l}{\partial t} - \nabla \cdot \left(\frac{RTt_1}{F^2} \frac{p_C \kappa(c_l)}{c_l} \nabla c_l + \frac{t_1 p_C \kappa(c_l)}{F} \nabla \phi_l\right) = 0 \tag{4.3}$$

$$- \nabla \cdot \left(\frac{RT}{F}(2t_1 - 1) \frac{p_C \kappa(c_l)}{c_l} \nabla c_l + p_C \kappa(c_l) \nabla \phi_l\right) = 0 \tag{4.4}$$

In the equations above it can be seen that in the electrolyte not only the concentration gradients are affected by the electrolyte conductivity κ, but also the gradient in the electrical potential, since the ions carry both mass and charge. So, κ is the main influence factor for transport in the electrolyte. This parameter gets scaled, when the cathode porosity p_C is changed. In addition to this, a change in p_C also changes the capacity of the electrolyte, namely the number of Li-ions that can be located therein. A test series has been performed in order to investigate, how different p_C values affect the cell behaviour, although measurement data for this quantity was available. The calculations done in section 3.3.3 resulted in a cathode porosity of about 80 %. This value means that 80 % of the electrolyte space in the cathode geometry are actually electrolyte and the rest is covered by binder and additives. This value in the series was varied from 5 % (nearly no electrolyte) to 100 % (pure electrolyte).

Fig. 4.7 depicts the simulation results. It can be seen that high porosity

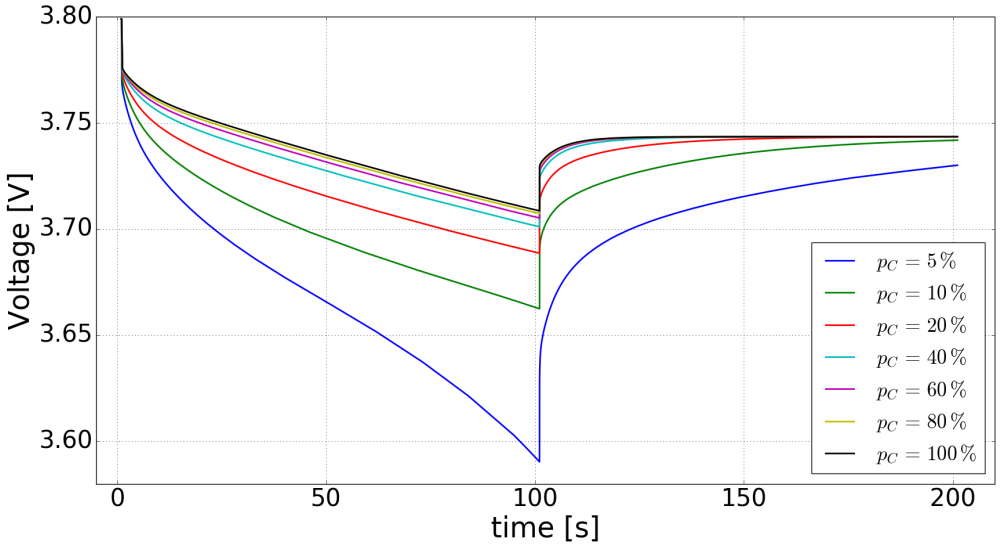

Figure 4.7: *Cell voltage for different values of the cathode porosity p_C, reaching from 5 % to 100 %. For a high cathode porosity $>$ 40 % the results are very similar. When the share of additives and binder exceeds 60 % the voltage drop gets larger over the course of the discharge pulse.*

values ($p_C > 40\,\%$) are very similar, with a low voltage drop throughout the discharge pulse and a fast relaxation into equilibrium after switching the current off. If the porosity gets lower which means that the fraction of additive and binder in the electrolyte regime of the cathode gets higher and thus the transport of ions is impeded, the voltage drop, as well as the relaxation times, significantly increase. The largest difference can be seen between the curves for p_C values of 10 % and 5 %. For the 5 % case the slope of the voltage curve increases with the time of the electric current flow, whereas it can be seen as approximately constant for all other cases. The cell has not reached equilibrium after the 100 s of relaxation. Simulations with even smaller values of p_C, for instance 1 %, have been performed, but they failed, because transport in the electrolyte was nearly non-existent in these simulations. The overall voltage drop for the considered porosities can be seen in Fig. 4.8. A low value of p_C leads to a low ion conductivity and a low ion capacity in the electrolyte.

So the transport in the electrolyte part of the cathode is much slower and less ions are available because of the lower capacity than for a high p_C value. This in turn has a big influence on how the particles are filled in the cathode. A segment of the cathode which depicts the situation in the cell is shown in Fig. 4.9. The image was recorded a few seconds after the current was switched on. The smooth area is the electrolyte with cubic particles inside it. In Fig. 4.10 the Li-ion gradients in electrolyte and particles along the x-axis corresponding to this geometry are shown.

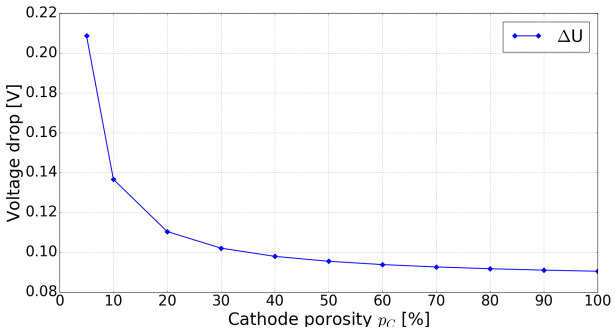

Figure 4.8: *Comparison of the overall voltage drop for simulations with different p_C values.*

The Figs. 4.9 and 4.10*b* show, how the slow transport in the electrolyte regime changes the way, the Li-ions enter the particles during discharge. For the high porosity case (red line) in Fig. 4.10*b*, the concentration gradient in the particles is relatively small; the Li-ions were transferred into all particles in a similar way. A low porosity completely changes this behaviour. The particles which are nearest to the separator and thus the anode, have a high Li-concentration (red in the image), whereas particles farther away show a much lower ion concentration (blue in the image). The particles are in a way filled with Li-ions *"row by row""*. This can again be explained with the equivalent circuit diagram in Fig. 4.5. In the case of a low p_C value the resistances in the electrolyte are high and limit the transport of the ions. They again will follow the path of the lowest overall resistance. In this case nearly all of them will go over the first particle, until the concentration there has reached a high value and its resistance has become so high that it is

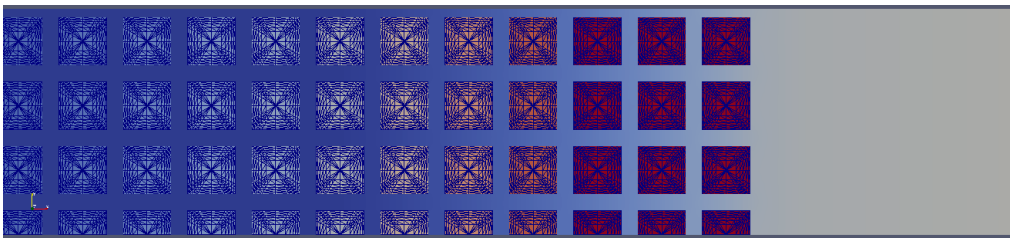

Figure 4.9: *Segment of the cell geometry for $p_C = 10\,\%$. The smooth area is the electrolyte with the cubic particles inisde. The low porosity leads to a slow transport in the electrolyte. The particles in the cathode are thus filled "row by row".*

easier for the ions to go over the second particle and so on. This is exactly the situation we see in Fig. 4.10*b*. The particles in the high p_C case are all filled similarly, with a slightly higher concentration near the separator. For the low p_C case there is a much larger difference in the particle concentrations, when going further away from the separator.

Fig. 4.10*a* shows the Li-ion concentration in the electrolyte across the x-direction. The porosity in the separator is 50 % for both cases, so the differences occur in the cathode only. For the low porosity case (blue line), a drastic drop in the Li-ion concentration can be observed due to the reduced capacity compared to the separator. The red line shows the case with pure electrolyte without any additives or binder. At the beginning of the discharge pulse the Li-ion concentration is the same over the whole cell. In both cases the same amount of Li-ions is extracted from the electrolyte and transferred into the particles, since the current is a fixed quantity. In the low p_C case this has a much larger influence on the concentration since the overall amount of electrolyte in the cathode is much lower. When the current continues to flow, more and more available ions in the electrolyte react and get transferred into the particles. The cell behaviour for $p_C = 10\,\%$ is further inhibited since not only the capacity of the electrolyte region is reduced, but also the conductivity. So *"fresh"* Li ions coming from the anode will be transported much slower which is another reason for the high electrolyte

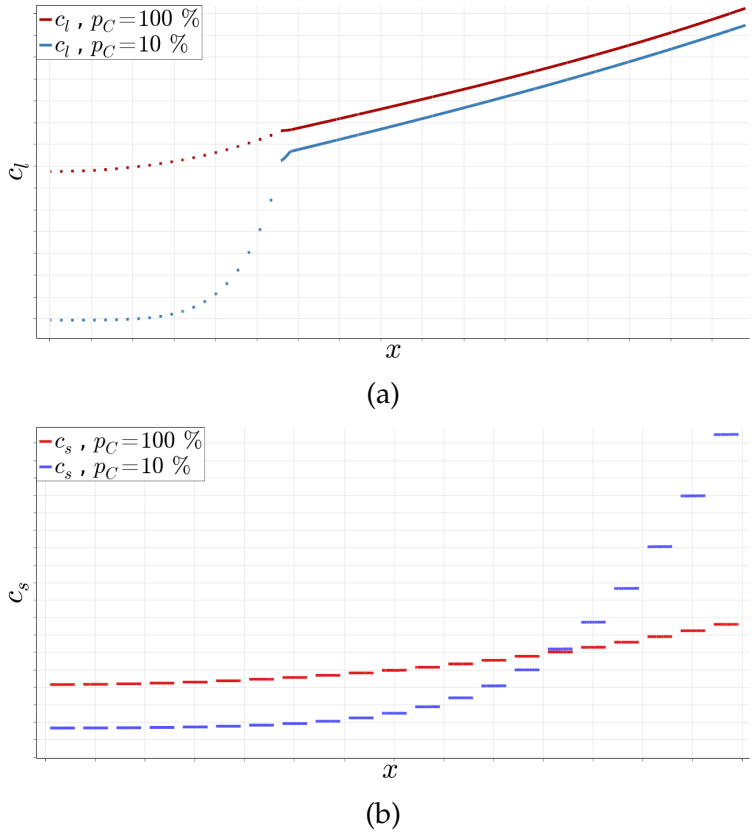

Figure 4.10: *Li-ion gradients in electrolyte and particle for $p_C = 100\,\%$ (red) and $p_C = 10\,\%$ (blue) along the cells x-axis.* ***a.)*** *Electrolyte concentration gradient* ***b.)*** *Particle concentration gradient*

resistance. The gradients in the concentration for the low porosity case get thus even bigger, when the discharge current flows for a longer time. After switching the current off, the process gets inverted and the gradients start to diminish. The high porosity case reaches equilibrium already after a few seconds, whereas the gradients have not fully disappeared for the low porosity case after the full $100\,s$ relaxation time. In section 4.1.1 the gradients inside the particles were the inhibiting the relaxation. In this case the relieve of the gradients in the electrolyte is so slow that it prevents

the system from reaching the equilibrium voltage after the relaxation time in the simulation. In addition to this there are also still small gradients between the particles which indicates that the low electrolyte conductivity also prevents the balance of the concentration on the particle side. If these results are compared to the ones obtained from the D_0 variation, similarities in the impact, these two parameters have, can be seen. The shape of the curves changes in a similar way as the parameters are set to lower values. An explanation may be that both directly affect the transport of the Li-ions, D_0 in the particles and p_C, κ, in the electrolyte and that a hindrance of the Li-ion movement in the particle or in the electrolyte leads to a similar influence on the cell voltage. Both of these transport parameters affect the additional voltage drop that occurs, when a current flows for a longer time. The calculated value of $p_C \sim 80\,\%$ lies in the regime, where small deviations from the value have nearly no influence on the cell voltage. To really see differences in the cell voltage, this value would have to be much lower and the results from the calculations are far away from values which could be critical for the cell behaviour.

4.1.4 Variation of the Initial State of Charge *SoC*

In Tab. 4.6 the parameter specifications for the test series are shown. Geometry and current profile used are described in Tab. 4.1. The *SoC* influences many aspects of the model, such as the OCV, i_0 and D_s.

Parameter	Value
D_0	10^{-10}
k_{BV}	10^{-3}
p_C	80 %
SoC	**20 - 100** %

Table 4.6: *SoC* test series specifications

Every simulation needs an initial state of charge *SoC* of the cell as an input. Throughout the calculated profile this value changes, depending

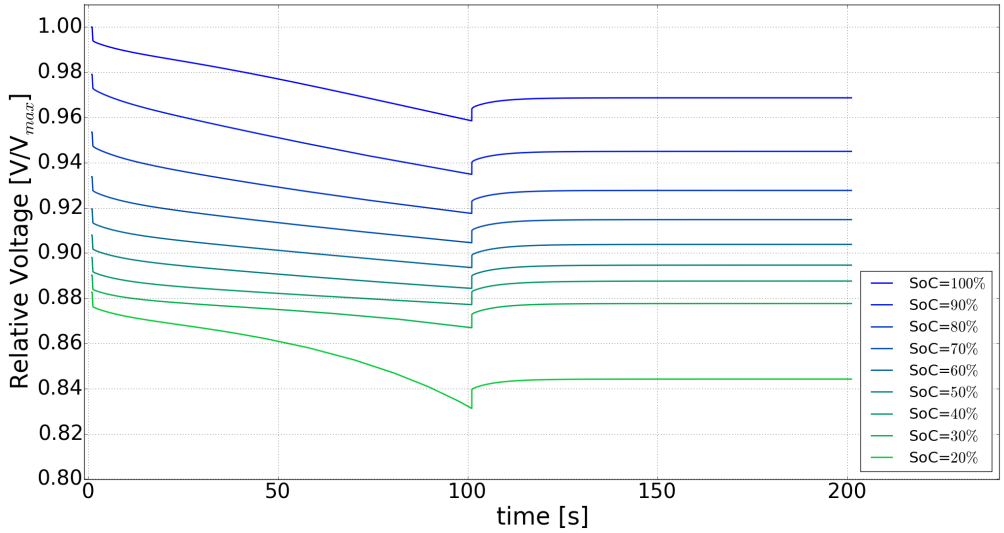

Figure 4.11: *Simulation results for different SoC values. The voltages are relative values compared to the maximum voltage. It can be seen that a lower initial SoC means a lower starting voltage. In addition to the voltage level, the form and the voltage drop are affected as well by the SoC.*

on whether the cell is charged or discharged. How the *SoC* affects the OCV and in further consequence other quantities in the model, has already been explained in section 2.7. A test series has been performed in order to quantify this influence. The *SoC* was varied from a low value of 20 % up to a fully charged cell with 100 %. A lower starting value was not possible, due to the length of the discharge pulse and its current. A 100 s discharge pulse with 5 C leads to a decrease in the *SoC* of about 15 %. For an initial value lower than 20 % the *SoC* would go near zero or even drop below zero which cannot be simulated, because negative *SoC* values which would correspond to an overdischarge, are not considered in the model. The other selected parameters which were varied in the section before, were fixed at relatively high and uncritical values, so their influence on the cell behaviour could be viewed as small.

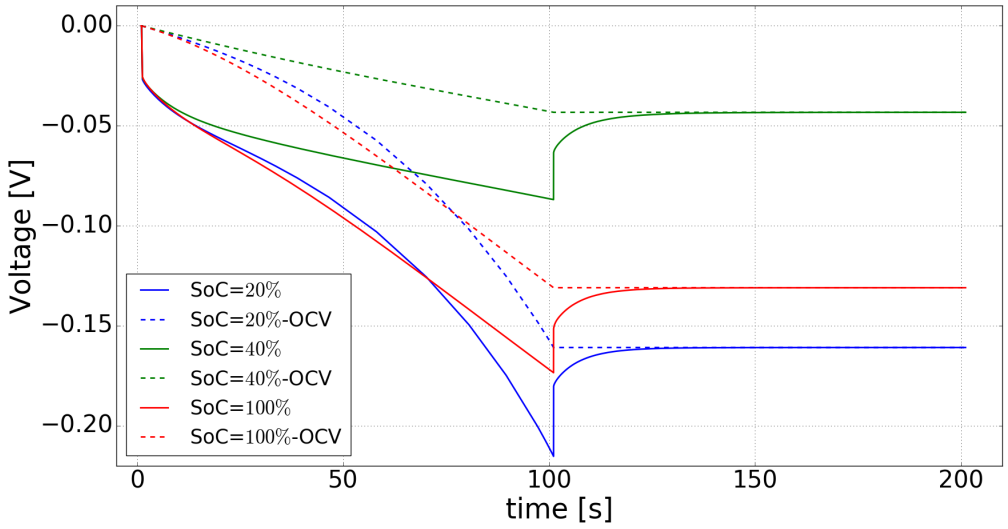

Figure 4.12: *Plot of selected curves for* 20 %, 40 % *and* 100 % *SoC.The full lines show the simulation results; the dashed lines represent the pure OCV contribution.*

Fig. 4.11 shows the results of the model calculations for the different *SoC* start values. The voltages are displayed as relative values compared to the maximum voltage occurring in the figure. The first thing that can be seen is that the starting voltage of the pulse is different for all *SoC* values. This is due to the fact that this initial cell voltage is taken from the OCV curve of the cell which is a function of the *SoC*. The more charged the cell, the higher its cell voltage. Since the OCV is not a straight line, the differences in the initial cell voltage for a 10 % *SoC* difference are not constant. From plotting these initial voltages, together with the voltages at the end of the relaxation time, an approximation of the OCV could be reconstructed. An example for a OCV curve was already shown in Fig. 2.7.

The *SoC* does not only affect the initial voltage level, but also the voltage drop over the course of the pulse and the shape of the discharge curve. As can be seen, the curve for a *SoC* of 20 % has a higher voltage drop than the ones with higher *SoC* values. Three selected curves for 20 %, 40 % and

100 % SoC have been chosen to show these differences in shape and the magnitude of the voltage drop in more detail. For this purpose, the initial voltage value was subtracted from all curves in order to assure that they all start at 0 V. The results are plotted in Fig. 4.12. The full lines correspond to the simulation results. For the curves with different SoC values, one has to distinguish between the voltage drop that occurs only due to the changes in the SoC (ΔSoC) during the simulations, in other words, the contribution from the OCV, and the voltage drop that is due to overpotentials. For this purpose the voltage progress due to ΔSoC only, was included in the figure separately using dotted lines. It can be clearly seen that the OCV contribution has a significant influence on the voltage behaviour and the shape of the curve throughout the discharge pulse. The voltage drop is not caused by overpotentials only. When comparing the dotted and the full lines, one can see that the basic shape of the discharge curve is determined by the ΔSoC part which is significantly different for all three considered pulses. Especially the 20 % case (blue) differs from the other curves, because in this SoC region the OCV curve has a higher slope and differences in the SoC thus have a greater impact on the voltage than for higher SoC values. This distinction between the OCV contribution and the overpotential to the total voltage drop holds for all simulations considered in this thesis, but because in the previous sections the initial SoC was not changed, its influence was the same for all cases. The difference between the full and the dotted lines is the contribution of the different overpotentials. One can see that the initial voltage drop is not SoC dependent, it is the same for all three curves and relatively small, due to the high k_{BV} value. The further progress of the curves is relatively parallel to the OCV curves which indicates that the other, transport-related overpotentials, as diffusion inside the particles and the electrolyte, are small. This is as expected, since the values of D_0 and p_C were set to non-critical values.

In Fig. 4.13 the total voltage drop over the full discharge pulse is plotted versus the *SoC* value of the simulation. As already discussed the voltage drop is higher for nearly discharge and for fully charged cells and it is lower for intermediate values of the *SoC*, with a minimum at about 40 % *SoC*. This again can be explained by the shape of the OCV curve and the *SoC* dependence of the model parameters D_0 and i_0. Analysing the results in **Paraview**, it can be seen that the level of the Li-ion concentration in the particles is proportional to the *SoC* value. The lower the *SoC*, the more ions are intercalated in the cathode. The basic cell behaviour, however, that is how the particles are filled, and how the Li-ion concentration gradient in the electrolyte evolves, are very similar for the different cases. This is because all other model parameters were set to high values, so the charge transfer and the transport in the cathode are fast.

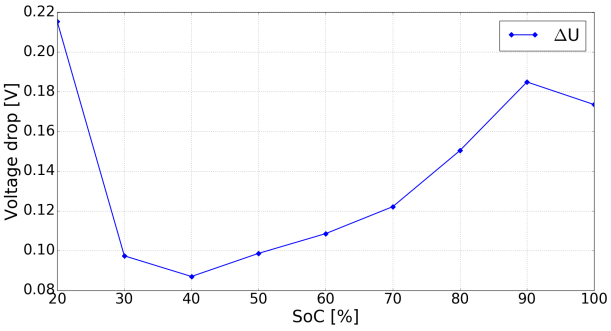

Figure 4.13: *Plot of the overall voltage drop versus the initial SoC. It shows a minimum for SoC* $\sim$ 40 %.

4.2 Parameter Cross Effects

Now that the isolated influence of each selected parameter on the cell behaviour and the cell voltage has been investigated, it is assumed that the parameters mutually influence each other. In order to analyse this issue, additional simulations have been performed, where more than one parameter has been changed at once. The influence of the *SoC* on different

values of the cathode side reaction constant k_{BV} and the cathode porosity p_C is analysed in the sections 4.2.1 and 4.2.2.

An important parameter that has not been changed up to this point, but is assumed to have a major impact on the whole simulation, is the C-rate of the discharge pulse. A higher C-rate means a higher current extracted or introduced from/into the cell during discharge/charge. In order to investigate the influence of the C-rate on the simulation results, a new input current profile, as described in section 3.4.2 and shown in Fig. 3.6*b*, consisting of a series of three discharge pulses has been used. In section 4.2.3 the results for the different C-rates, together with a variation of D_0, k_{BV} and the *SoC*, will be compared.

4.2.1 Variation of k_{BV} and *SoC*

In Tab. 4.7 the parameter specifications for the test series are shown. Geometry and current profile used are described in Tab. 4.1. Two different k_{BV} values were investigated for three different *SoC* values.

Parameter	Value
D_0	10^{-13}
k_{BV}	**10^{-3}, 10^{-9}**
p_C	80 %
SoC	**20, 50, 100 %**

Table 4.7: Specifications for the k_{BV} & *SoC* test series

In this series, cross effects between the cathode reaction constant k_{BV} and the *SoC* have been investigated. These cross effects are assumed to exist, since in the governing equations the exchange current density i_0 depends on the *SoC*, as it has been shown in section 2.7. To prove this assumption, the simulation has been run several times at three different *SoC* values (20, 50, 100 %) and two different k_{BV} values (10^{-3}, 10^{-9}). The diffusion coefficient D_0 and the cathode porosity p_C were held constant. In Fig. 4.14 the results obtained

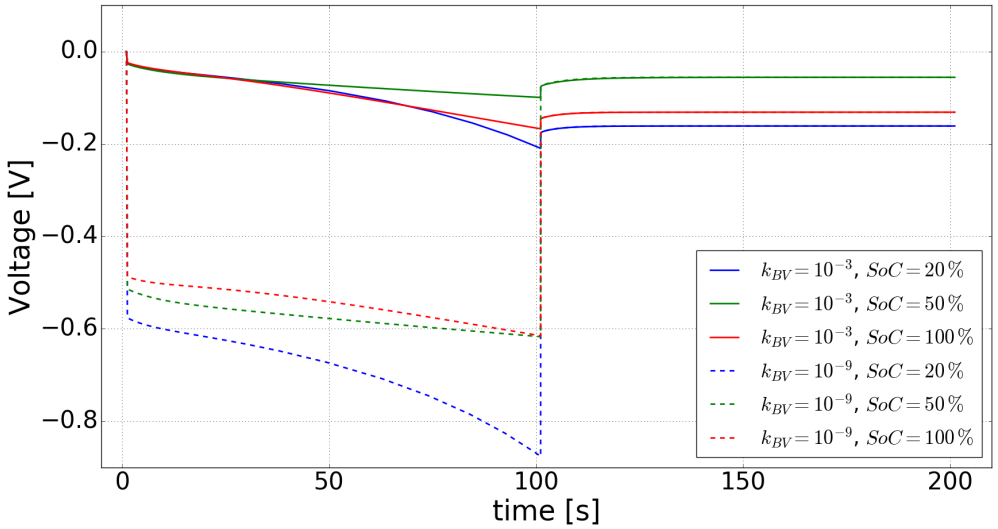

Figure 4.14: *Simulation results for different values of the SoC and k_{BV}. For $k_{BV} = 10^{-9}$ (dashed lines) the SoC influences the initial voltage drop. For $k_{BV} = 10^{-3}$ this influence is negligible.*

from these simulations are shown. The dashed lines represent the results for the low k_{BV} value.

For $k_{BV} = 10^{-3}$ the results are as already obtained from Fig. 4.12, with a 50 % *SoC* pulse instead of a 40 % pulse. The lower diffusion constant of $D_0 = 10^{-13}$ has only negligible influence. The overall voltage drop depends on the *SoC* and it is lowest for the medium *SoC* of 50 %. For $k_{BV} = 10^{-9}$, however, a new effect can be observed. As can be seen in the figure the initial voltage drop is not the same for the three different curves although the k_{BV} value is the same. So the initial voltage drop is not only dependent on k_{BV}, but also on the *SoC*. This dependence gets bigger, the lower the value of k_{BV} becomes which is why it could not be observed in the previous section. In the other case, small differences are observed, but the high reaction constant in a way superimposes the *SoC* influence. This shows the two parts this initial voltage drop consists of. There is on the one hand the contribution

of the electrolyte which is not SoC dependent and is always present. On the other hand there is the contribution of the charge transfer resistance which is determined by k_{BV} and is depending on the state of charge. The magnitude of this additional SoC dependent contribution gets higher, the lower the SoC value is. For a low SoC, the ion concentration in the particles is high. There is an additional resistance for an ion to enter a particle. This affects not only the initial voltage drop, but also the further voltage drop as the discharge pulse proceeds. It is much higher for the low k_{BV} value, as can be seen if the two 20 % SoC curves are compared. The 50 % and the 100 % results in a very similar voltage at the end of the pulse, although it is not exactly the same. The voltage drop for the 100% curve is higher, as expected, but the initial voltage drop is lower, so they both end up at nearly the same value. The voltage jump at the beginning of the relaxation is such that the curves result at a value dependent on their SoC, but not on k_{BV}. This complies with the results from section 4.1.2, where the relaxation did not depend on k_{BV} either. Since the diffusion constant for these simulations was at an intermediate value, the relaxation is fast and the cell reaches its equilibrium voltage right after switching the current off.

4.2.2 Variation of p_C and SoC

In Tab. 4.8 the parameter specifications for the test series are shown. Geometry and current profile used are described in Tab. 4.1. Different values of p_C were investigated at three different SoC values.

Parameter	Value
D_0	10^{-13}
k_{BV}	10^{-3}
$\boldsymbol{p_{El}}$	**10 - 50** %
SoC	**20, 50, 100** %

Table 4.8: Specifications for the p_C & SoC test series

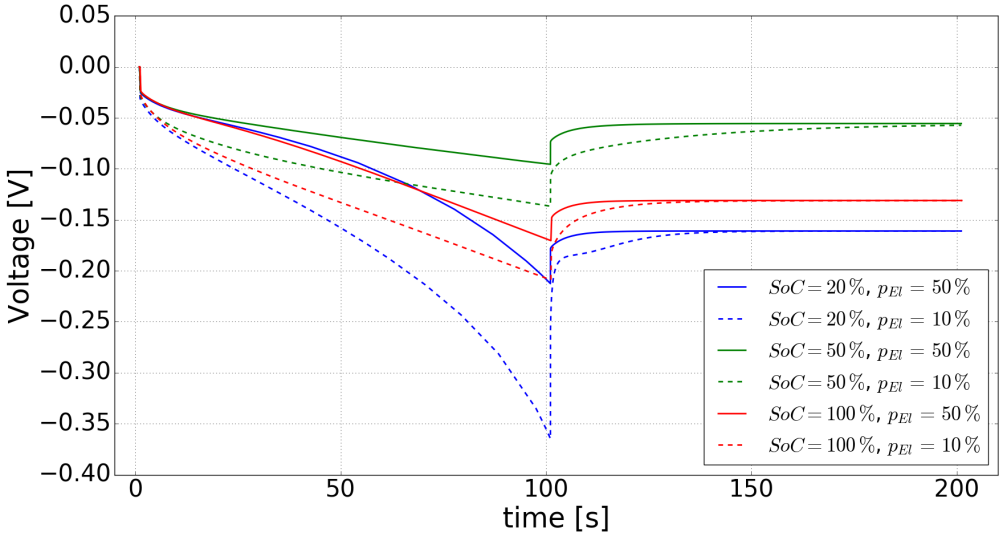

Figure 4.15: *Simulation results for different values of the SoC and p_C. The full lines show the $p_C = 50\,\%$ case, the dashed lines are the results for $p_C = 10\,\%$.*

In section 4.1.3 the impact of the cathode porosity p_C has been studied. It was shown that this parameter mainly influences the shape of the voltage curve after the initial voltage drop. In this section the simulations for selected values of p_C are repeated for different *SoC* values, namely for 20 and 50 % *SoC*.

In Fig. 4.15 the simulation results are shown. The behaviour for the $p_C = 50\,\%$ curves (full lines) is already well known from section 4.1.4, again with a 50 % *SoC* pulse instead of a 40 % pulse. The dashed lines show the results for the same simulations with three different *SoC* values, but with a cathode porosity of only 10 %. The difference between the curves is significant, especially for the 20 % *SoC* case. As expected, the negative effects of the low *SoC* and the small value of p_C sum up and lead to a even worse cell behaviour. For a small value of the cathode porosity and a low *SoC* the overpotential needs to be very high in order to keep the current up. Due to the low p_C the ion can move only very slowly in the electrolyte and due

to the low SoC the particles are already filled with Li-ions. When looking again at the equivalent circuit diagram in Fig. 4.5 in this specific case the resistances in the electrolyte are high due to the low p_C and the particle resistance is high as well due to the high Li-ion concentration because of the low SoC. The effect of p_C on the higher SoC cases is much lower which can again be explained with the Li-ion concentration inside the particles. In the equivalent circuit diagram the particle resistances are lower and thus the overpotential is not that high. As presented in section 4.1.3 for a high cathode porosity all particles will get filled similarly, whereas for the low value the particles will get filled row by row due to the high electrolyte resistance.

4.2.3 Triple Pulses - Variation of the C-Rate

In Tab. 4.9 the parameter specifications for the test series are shown. Geometry and current profile used are described in Tab. 4.2. The varied parameters were D_0, k_{BV} and the SoC.

Parameter	Value
$\boldsymbol{D_0}$	$\mathbf{10^{-10}}$ **-** $\mathbf{10^{-15}}$
k_{BV}	10^{-3}
p_C	80 %
SoC	**20, 50, 100** %

Table 4.9: Specifications for the C-rate test series

Up to this point in the thesis the current input profile for all simulations was chosen to be a single discharge pulse with a fixed current of 5 C. The C-rate which defines the charge or discharge current, has a strong influence on the cell behaviour. It makes a difference, if the cell is charged/discharged with a high or with a low current. For the purpose of the investigation of this issue, a new current profile has been created. Instead of a single discharge pulse, three discharge pulses with different currents of 0.5, 2.5 and 5 C, are subsequently simulated. To allow a comparison of the pulses, the initial

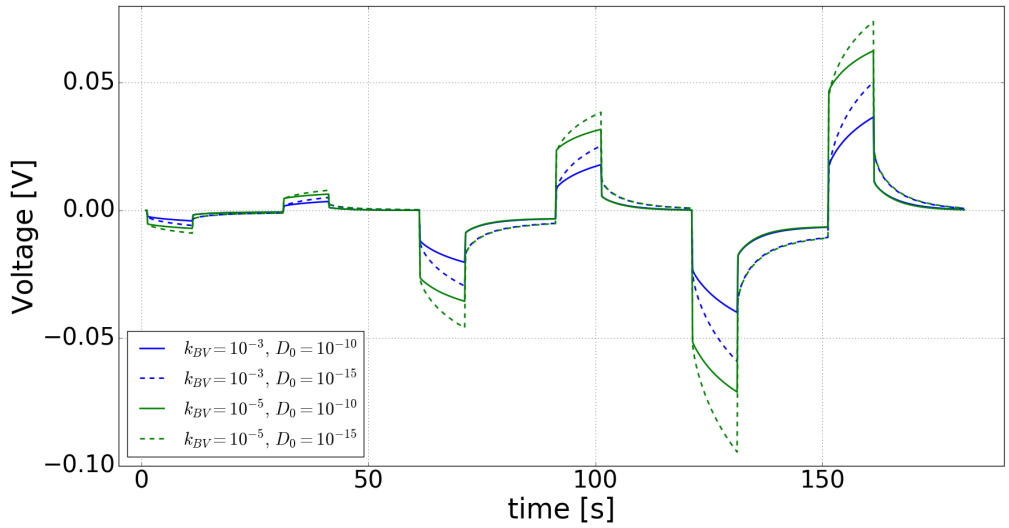

Figure 4.16: *Resulting voltage curves for a triple discharge/charge input current profile for two values of k_{BV} and D_0. It can be seen that a higher current enhances the influence of the parameters.*

SoC of each pulse has to be the same. To assure this each discharge pulse is followed by a charge pulse of the same current to recreate the initial *SoC*. Every pulse is separated by the following pulse by a 20 s relaxation period. Each pulse is 10 s long. In addition, this simulation was run several times with different values of D_0, k_{BV} and the initial *SoC* in order to investigate, how the parameters behave at different currents. Since the simulations so far have been performed with a high discharge current, in this section it will be shown, how the results change for a lower current.

Simulation results for different k_{BV} and D_0 values can be seen in Fig. 4.16. The full lines correspond to the simulations with $D_0 = 10^{-10}$; the dashed lines to $D_0 = 10^{-15}$; the blue curves show the results for $k_{BV} = 10^{-3}$; the green ones for $k_{BV} = 10^{-5}$. The pulses with a negative voltage drop correspond to the discharge pulses, the ones with a positive voltage change to the charge pulses. All pulses have been recalculated to start at 0 V. What

can be seen immediately is that the voltage drop is directly proportional to the C-rate. The higher the current, the higher the SoC change of the cell in the same discharge time. The larger the difference in the SoC, the larger the difference in the corresponding OCV value. This affects also the influence of the other parameters, such as the exchange current density i_0 which is mainly responsible for the initial voltage drop, as well as the diffusion coefficient D_s which determines the voltage drop over the course of the discharge pulse. As shown in section 4.2.2, also the cathode porosity p_C which scales the electrolyte properties, is dependent on the SoC and thus affected by the C-rate. In these simulations however it was set to an uncritical value, so its influence is small. The relaxation after switching the current off for the low diffusion case, is short for the pulses with 0.5 C and gets significantly higher for the other two pulse series. This is because for a higher current, larger gradients get established which take longer to relieve. The cell is farther away from the electrochemical equilibrium. Another interesting observation that can be made, is the charge and discharge pulses with the same current are not symmetric. For instance the voltage change for the 5 C discharge pulse with $D_0 = 10^{-15}$ is ~ 0.9 V, whereas it is only ~ 0.7 V for the corresponding charge pulse. This difference is present for all curves and gets larger for higher currents and lower diffusion constants. This discrepancy does not occur for the high diffusion case. It can be explained by looking at the relaxation times of the pulses. After the discharge pulse the system has not gone reached electrochemical equilibrium for the $D_0 = 10^{-15}$ case. In section 4.1.1 it was shown that for a slow diffusion, the Li-ions accumulate at the particle surface and that the gradients inside the particles cause the slow relaxation. The gradients were not fully relieved after a 100 s relaxation period. In this case there are only 20 s of relaxation and the system is far away from electrochemical equilibrium. This means that at the particle surfaces there is still a much higher concentration, than in the particle centres. When a charge current is applied, Li-ions get extracted

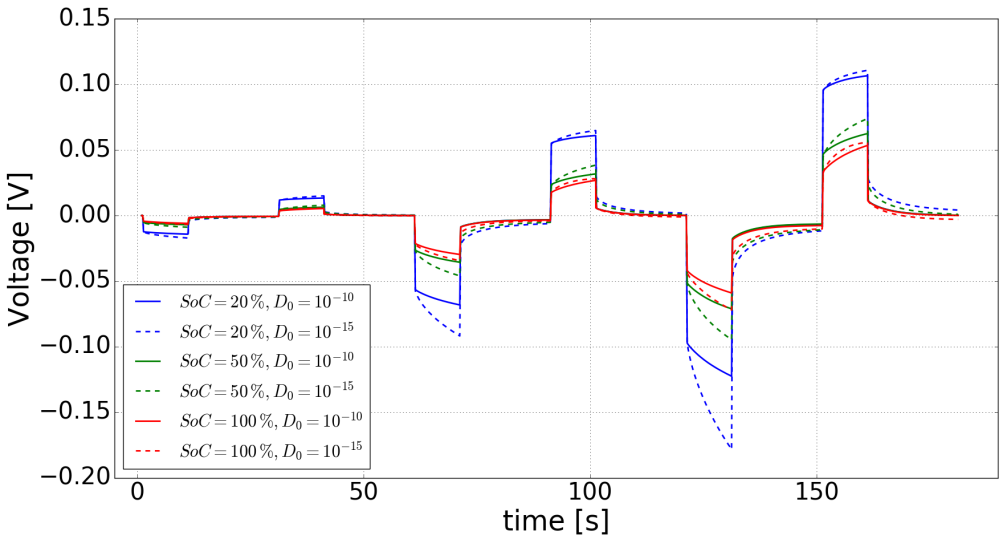

Figure 4.17: *Resulting voltage curves for a triple discharge/charge input current profile for different values of SoC and* D_0.

from the cathode particles and move towards the anode. Because of the high surface concentration the influence of the slow diffusion is not that relevant. The Li-ions do not have to diffuse over long distances, because they are already at the surface and can react immediately. This effect also gets stronger for higher currents and is present for both k_{BV} values.

Next the *SoC* has been varied and results for two values of D_0 (again 10^{-10} (full lines) and 10^{-15}(dashed lines)) are compared in Fig. 4.17. Three values of the *SoC* have been looked at (20 (blue), 50 (green) and 100 % (red)). The voltage drop is directly proportional to the *SoC* of the cell. It is lowest for the fully charged cell and gets higher with decreasing *SoC*. This corresponds to the results obtained in section 4.2.1. Although the voltage drop is higher both for very low and very high values of the *SoC*, the *SoC* dependent contribution to the initial voltage drop superimposes this effect and leads to the results seen here. The 50 % and 100 % curves are quite similar, whereas the 20 % curve shows a much worse cell behaviour. The discrepancy in

voltage change between discharge and charge pulse can also be seen here. The reasons are the same as explained above. The difference between low and high diffusion gets higher, the lower the SoC is. This can be explained with the Li-ion concentration in the particles and the SoC dependence of the model quantities i_0 and D_0. When the particles are nearly filled with Li-ions, a higher overpotential is necessary to assure that enough Li-ions get transferred into the particles in order to keep the current up. If one looks at the relaxation times for the low diffusion cases, one can see that the cases with higher SoC relax faster into an equilibrium state, although none of the three curves has reached the equilibrium after the 20 s of relaxation.

4.3 Influence of the Geometric Arrangement

One important scope of this thesis is also the investigation of the influence of the geometric arrangement of the active material particles in the cathode on the behaviour of the cell. In order to tackle this specific goal, every simulation of a single discharge pulse of 5 C which has been reported here has actually be done twice with two different geometric arrangements in the cathode; once for particles distributed equally over the whole cathode and once for aggregated particles, with small distances between the particles inside an aggregate and large distances between the aggregates. The differences and specifications for the geometries have already been explained in section 3.4.4 and examples were shown in Fig. 3.7. In this section, the results of the analysis of this data will be presented. Before showing the results, it has to be noted that by choosing the cell geometry for the simulations, one quantity has been fixed already at the beginning, namely the ratio between active material particles and electrolyte region in the cathode. It is determined by the size of the cathode and the side lengths and the number

of the particles. In the geometry used, this value was about 55 %, so more than half of the cathode box was covered by particles. This ratio was held constant and in the following it will be shown, whether the two different arrangements of the particles in the cathode lead to significant differences in the cell behaviour. Further it will be investigated, how the change of the physical model parameters enhances or attenuates these differences. The parameters will be discussed one by one.

Solid Diffusion Coefficient D_0 This parameter influences the movement of the ions inside the particles in the cathode. When simulating a discharge pulse, a low value of D_0 leads to a larger voltage drop throughout the course of this pulse. When looking at a geometry with aggregated particles, as can be seen in Fig. 3.7*b*, it is expected that the ions are hindered to get into the small pores between the aggregated particles. Since D_0 does not influence the ions before they reach the particles this quantity is not expected to drastically influence the cell behaviour for different geometric arrangements. Analysis of the simulation results confirms this assumption. The difference in voltage between the aggregated and the equally distributed geometry was $< 1\,mV$ for both high and low values of D_0.

Cathode Reaction Constant k_{BV} The order of magnitude of k_{BV} scales the exchange current density in the BVE. It determines, how big the resistance for the Li-ions is, when they react at the interface between particle and electrolyte in the cathode. When the particles are aggregated, the pore size inside an aggregate is very small. The resistance for the ions to reach the particle interfaces inside an aggregate will be higher than for the equally distributed particles. But when an ion reaches the interface, the reaction will occur independently of the geometry. When comparing the simulation results for both cases it can be stated that the influence of k_{BV} on the

difference in cell voltage between the two geometries is small. The voltage differences are again below $1\,mV$, both for high and low values of k_{BV}.

State of Charge SoC The initial state of charge of the cell before starting a simulation has, besides the actual voltage level, a big influence on many aspects of the cell behaviour, especially on the voltage drop throughout the pulse. It determines the Li-ion concentration in the particles. The higher it is, i.e. the lower the SoC, the more difficult it is for additional ions to enter the particles. Again this value does not have a major impact on how the ions get to the particles. The difference between the two arrangements is larger for low SoC values and gets smaller, as the SoC increases. The magnitude of this difference, however, is negligibly small, i.e. below $1\,mV$ even for the 20 % SoC simulations.

Cathode Porosity p_C The value of this parameter determines how much space of the electrolyte in the cathode is covered by additives and binder material, and thus the magnitude of the ionic conductivity in the electrolyte. A low porosity value means that the electrolyte space is clogged with those additives and binder and the movement of the ions is hindered. This means in further consequence that they will move much more slowly through the electrolyte and in the case of an aggregated geometry, this may prevent a significant number of ions to get into the small pores between the aggregated particles which in turn may cause a worse cell behaviour, than for the equally distributed particle geometry. Fig. 4.18 shows the simulation results for 5 C discharge pulse for p_C values of 5, 10, and 20 % for equally distributed particles (full lines) and particle aggregates (dashed lines). Indeed it proves the assumption made above. Whereas for the 20 % case the differences are again relatively small, significantly worse behaviour for the aggregated geometry can be observed for the two cases with a lower p_C value. One has

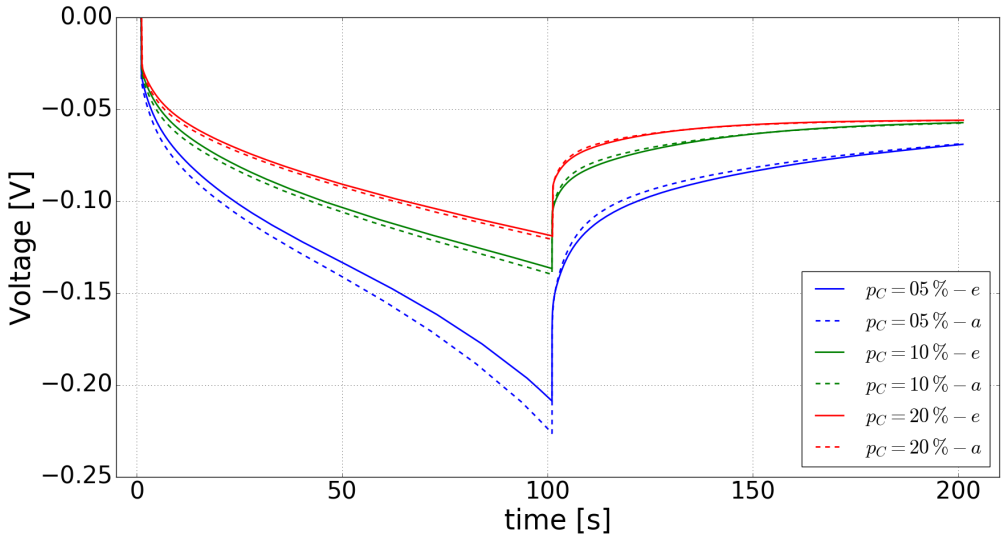

Figure 4.18: *Comparison between the discharge curves for equally distributed particles and particle aggregates for three different p_C values. For low cathode porosities significant differences in the cell voltages can be observed.*

to note that $p_C = 20\,\%$ is still a low value and the difference is still bigger than $1\,mV$ which was the maximum value obtained from the variations of the other parameters which all were calculated with a p_C value of 80 %. To see how the geometric difference depends on the value of p_C the minimum voltages of the two geometry cases have been compared and their difference was plotted over the specific p_C values which can be seen in figure 4.19. It is shown that the voltage difference raises massively for p_C values below 20 % and saturates at a value of about $1\,mV$ for higher values. So for a low p_C value there is a significant difference between the two considered geometries.

If the data is analysed and compared in Paraview, the differences in the behaviour can be made visible. In Fig. 4.20 the Li-ion concentration gradients in electrolyte and particle across the x- and y-axis are shown. The x-axis, in this case, goes from cathode to anode and cuts through the centre particle

row. The y-axis here cuts through the centre row of the second aggregate, respectively the corresponding particle for the equal geometry. The red lines correspond to the case with equally distributed particles, the blue lines to the case with particle aggregates. For both cases p_C had a value of 10 %. The images have been recorded a few seconds after switching the current on. In Fig. 4.20*a* the Li-ion concentration in the cathode electrolyte region can be seen. The lines represent the space between the particles, because in the particles itself, the Li-ion concentration in the electrolyte is not defined. At the right-hand side there is the interface to the separator and both concentrations are similar. In both cases the concentration gradients are expected to be high, since $p_C = 10\,\%$ value means that the other 90, % of the electrolyte region (c_l) in the cathode are actually binder and additives, so the capacity and conductivity of the electrolyte is reduced. At the first particles reactions occur and the concentration in both cases drops. The drop for the aggregated case is even higher, since due to the low conductivity and the small pores, nearly no ions can get to the particles inside the aggregate. This can be seen as well for the other two aggregates. Here the concentration drop is not that big in the first second of the discharge, since the reactions tend to occur first at the particles nearest to the separator. This is also the reason why the concentration goes up a bit near the cathode current collector. When the discharge pulse proceeds, reactions will also occur at the particles farther away from the cathode and a very large gradient gets established, where

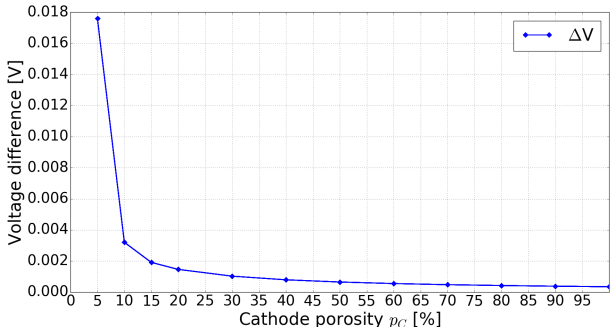

Figure 4.19: *Comparison of the difference in voltage drop between the two geometries for various p_C values.*

the concentration is highest near the separator and lowest at the rear side of the cathode. The additional drop inside the aggregates still can be seen.

In Fig. 4.20*b* the Li-ion concentration in the particles (c_s) across the x-axis is plotted. Here it can be observed as well that the particles in the aggregates which are not directly exposed to the bulk electrolyte have a lower concentration, because due to the small pores and the low conductivity it is much harder for the ions to reach these inner particles than the outer ones. Due to the small capacity a charge transfer into the particles has a much bigger influence on the concentration. The general behaviour is as already explained in section 4.1.3. Fig. 4.20*c* shows the Li-ion concentration in the particles across the y-axis. For the equally distributed particles no gradient can be seen. For the aggregated case, there is a noticeable gradient, even after only a few seconds of discharge. This indicates again that the inner particles of the aggregates are much harder to reach for the ions. The low conductivity and capacity enhance the geometric influence, since the slower the ions move, the more likely it is that they react at the first particle they encounter. As has been already mentioned above, the influence of the geometric arrangement was slightly higher for cells with a lower *SoC*. The difference however was very small which was assigned to the high p_C value which was used for the simulations. The same simulations for different initial *SoC* values of the cell were done again, but now with a very small cathode porosity of only 10 %. The results are shown in Fig. 4.21, where the differences in cell voltage between the two geometries is shown for the different *SoC* values. What can be seen is that the influence of the *SoC* on the geometrical differences is significant. For low *SoC* values the difference between the geometries is very large and it nearly goes down to zero for a fully charged cell. This can be explained by looking at the Li-ion concentrations in the particles. For a low *SoC* the value is very high, so the charge transfer into the particles for additional ions has a high resistance which leads to

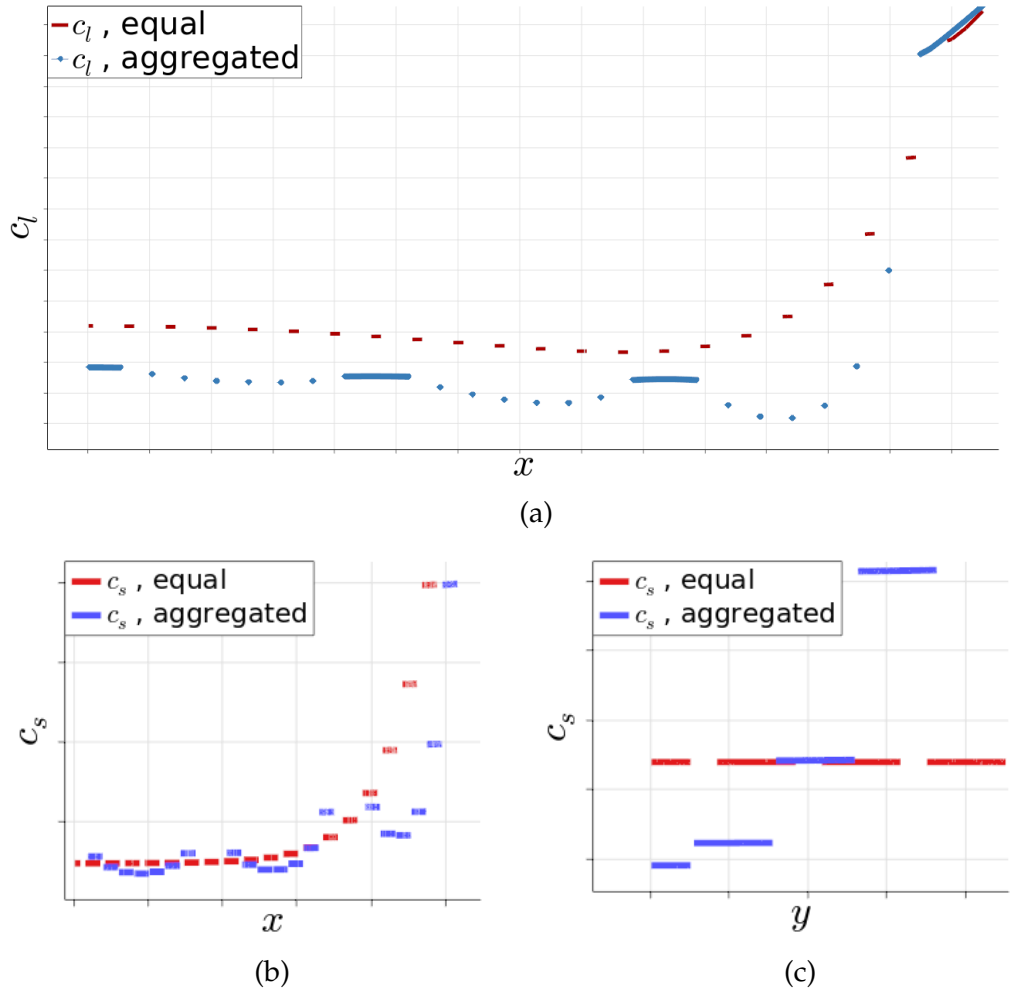

Figure 4.20: *Gradients across the x-axis and y-axis of the cell geometry. The red lines represent the equally distributed particles, the blue lines the particle aggregates* ***a.)*** c_l *across the x-axis of the cell.* ***b.)*** c_s *across the x-axis.* ***c.)*** c_s *across the y-axis*

a high overpotential in order to keep the current up. For a high *SoC* the Li-ion concentration in the particles is very low and the resistance for charge transfer is low. In this case the geometric arrangement is not that important, since enough Li-ions can react at the outer particles of the aggregate and do not need to go into the small pores. This is the reason why the differences in cell voltage for the two geometries become very small for high *SoC* values. So when there is little electrolyte available with a low conductivity, the influence of the *SoC* of the cell becomes much bigger than for cells with a high cathode porosity. In this study only the porosity of the electrolyte region has been varied, whereas the ratio between particles and electrolyte region was fixed. Here a tendency can be seen. When there is less electrolyte, the influence of the geometry gets bigger. It is expected that when putting more particles into the cathode, and thus their density gets higher and the total amount of electrolyte gets smaller, the geometric influence will be even enhanced.

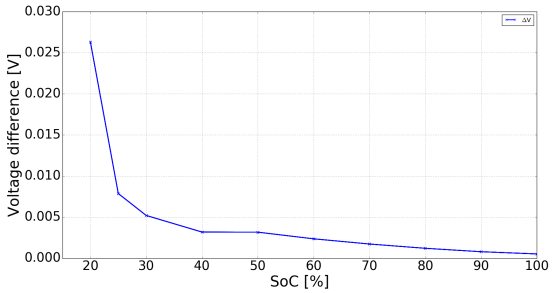

Figure 4.21: *Comparison of the difference in voltage drop between the two geometries for various SoC values for* $p_C = 10\,\%$.

Conclusion Simulations with two different geometric arrangements of the particles in the cathode, one with only one pore size, one with two distinguished pore sizes, have been performed. Several model parameters have been varied in order to find out which of them enhance or attenuate eventual differences between these two geometries regarding the simulation of a single discharge pulse. It has been shown that the influence of the

geometry for most of the simulations performed with uncritical values of the physical parameters can be considered small and the variation of most of the parameters does not alter this fact. The variation of the cathode porosity p_C however, revealed big differences in the behaviour of these geometries, when it is set to a very small value $< 20\,\%$. The smaller the value gets, the larger the geometric differences regarding the evolution of the cell voltage become. This influence gets further enhanced, when the cell is at a low SoC and nearly completely vanishes for a initially fully charged cell. So it can be concluded that the lower the conductivity and the capacity of the electrolyte are and the lower the initial state of charge of the cell, the more important the geometrical arrangement of the particles in the cathode becomes. It has to be noted though that the p_C value of $80\,\%$ which was calculated from measurement data, is much higher than the values for which significant geometrical differences occurred.

5 Summary and Outlook

Summary At the *VIRTUAL VEHICLE Research Center* an electrochemical battery model has been developed. The model describes the transport of Li-ions in the cathode and in the electrolyte. The anode is not modelled in detail. In this thesis, this model has been applied to specific cell geometries in order to investigate,

1. if the model provides physically reasonable results
2. how the physical model parameters as for instance the diffusion coefficient influence the cell behaviour
3. how different arrangements of the particles in the cathode influence the cell behaviour
4. how a variation of the physical parameters influences the differences in the results between different cell geometries

In order to perform the simulations cell geometries have been created. The geometries represent a simplified schematic of a real cell. Since the governing equations are solved by using the finite element method, the geometry must be separated into a finite number of elements. This is done with the software **Salome**.

For the simulations a current profile was chosen as an input for the model. For the parameter variation a single discharge pulse was chosen as profile.

The model calculates the cell voltage and the gradients in the Li-ion concentration in the electrolyte and the particles as well as the electrical potential in the electrolyte as a response to the input current.

The investigation of the cell voltage showed that the voltage drop is caused by two processes. At first there is an initial voltage drop which occurs immediately after switching on the current and vanishes, when it is switched off again. The second contribution of the voltage drop evolves with the duration of the discharge pulse. The variation of the physical parameters led to the conclusion that the first part is primarily influenced by the charge transfer across the interface between electrolyte and cathode particles; a smaller contribution is caused by the resistance of the electrolyte. The second part of the voltage drop is mainly due to the transport mechanisms of the Li-ions, namely diffusion and migration which are caused by gradients in the Li-ion concentration and the electrical potential respectively. Also the relaxation back to electrochemical equilibrium after switching off the current is influenced by the ion-transport more than by the charge transfer. In general it can be said, the slower the charge transfer and the transport, the larger the voltage drop in order to keep the current up. In addition pulses, with different initial values of the SoC have been investigated. The SoC has a significant influence on all aspects of the model, such as the OCV, the diffusion coefficient and the exchange current density. Fully charged and discharged cells show a higher voltage drop than cell with an intermediate SoC. For selected pulses the contribution of the OCV to the voltage drop has been calculated in addition in order to reveal the magnitude of the overpotential contribution.

It has been further investigated how the parameter mutually influence each other. As a result, it can be said that the SoC also affects the influence of the other physical parameters on the cell behaviour. In addition to the single discharge pulses, also a series of three discharge pulses with different C-

Parameter	ΔV Instant	ΔV Current	ΔV Geometry
D_0	✗	●	✗
k_{BV}	●	✗	✗
p_C	●	●	●
SoC	●	●	●

Figure 5.1: Summary of the influence of the varied parameters on the initial voltage drop, the voltage drop during the current flow and the geometrical differences. The red cross means negligible influence, the yellow circle means intermediate influence and the green circle indicates big influence.

rates has been simulated. In order to assure that every discharge pulse starts with the same *SoC*, it was followed by a charge pulse of the same magnitude. The discharge current is also primarily responsible for the voltage drop and enhances the action of all other parameters.

The geometrical influence was investigated by creating two different geometries, one with equally distributed particles, where the distance between the particles is the same in all directions, and one with particle aggregates with a small distance between the particles inside an aggregate and a large distance between the aggregates. It has been shown that the geometry has only a small influence on the cell behaviour for most of the performed simulations. But when the conductivity and the capacity of the electrolyte in the cathode are set to very small values, the aggregated geometry shows a much larger voltage drop than the equally distributed particles. For such a case the *SoC* has been varied in addition and it came to light that the geometric effect is strongly enhanced for almost discharged cells and vanishes nearly completely for a fully charged cell.

All achieved results are summed up in Fig. 5.1 in form of a descriptive table. Each investigated parameter is written in a row. The columns show the different issues discussed above, namely the contributions to the voltage drop and the geometrical differences. A red cross means negligible influence of the parameter, a yellow circle means an intermediate influence, and a green circle indicates that the parameter has a major influence on the specific issue.

Outlook After the plausibility of the simulation results has been confirmed, the model can be used to reveal new insights into the inner processes of a Li-ion battery. The systematic investigation of the influence of the geometric arrangement in the cathode has only just begun. The results achieved here stem from the investigation of two simple geometries. Parameters, like the number of particles in the cathode, the particle sizes, the external measures of the cathode, and the particle shape have all been fixed. Furthermore, for all the simulations regarding the geometric influence, a single discharge pulse has been used as an input and, for reasons of time and computational effort, all simulations were run on 2D geometries.

In future investigations for testing the applicability of the model all these parameters may be changed. What happens, when a cathode with much closer packed, but smaller particles, is used? What changes are to be expected when spherical particles with different sizes or a full 3D geometry are used for a simulation? All these questions will be tackled and will hopefully give a deeper understanding of the importance of the arrangement of the cathode particles which may provide useful informations to battery manufacturers in order for them to be able to further improve cathode materials.

Bibliography

[1] International Energy Agency. *WORLD ENERGY OUTLOOK 2015 FACTSHEET*. 2015.

[2] International Energy Agency. *WORLD ENERGY OUTLOOK 2015 Special Report: Energy and Climate Change*. 2015.

[3] British Petrol. *BP ENERGY OUTLOOK 2035*. 2015.

[4] United Nations-Department of Economic and Social Affairs. *World: Total Population*. 2015.

[5] European Commission. *Green Paper: A 2030 framework for climate and energy policies*. 2013.

[6] Energie-Control-Austria. *Statistikbroschüre 2015*. 2015.

[7] European Road Transport Research Advisory Council. *European Roadmap: Electrification of Road Transport*. 2012.

[8] European Road Transport Research Advisory Council. *European Roadmap: Infrastructure for Green Vehicles*. 2012.

[9] European Road Transport Research Advisory Council. *Energy Carriers for Powertrains*. 2014.

[10] Statista GmbH. *Projected market for lithium-ion batteries used in consumer electronics from 2012 to 2020 (in million U.S. dollars)*. 2015.

[11] Statista GmbH. *Projected market for lithium-ion batteries used in automobiles from 2012 to 2020 (in million U.S. dollars)*. 2015.

[12] Statista GmbH. *Size of the global market for electric vehicles in 2012 and 2019 (in billion U.S. dollars)*. 2016.

[13] C. Hamann and W. Vielstich. *Elektrochemie, 4.Auflage*. Weinheim: Wiley VCH, 2005.

[14] W. Schmickler. *Grundlagen der Elektrochemie*. Wiesbaden: Vieweg, 1996.

[15] A. Yoshino. "The Birth of the Lithium-Ion Battery." *Angewandte Chemie* 51 (2012), pp. 5798–5800.

[16] P. Van den Bossche, F. Vergels, J. Van Mierlo, J. Matheys, and W. Van Autenboer. "SUBAT: An assessment of sustainable battery technology." *Journal of Power Sources* 162 (2006), pp. 913–919.

[17] G. Ren, G. Ma, and N. Cong. "Review of electical energy storage system for vehicular applications." *Renewable and Sustainable Energy Reviews* 41 (2015), pp. 225–236.

[18] J. B. Goodenough and K. Park. "The Li-Ion Rechargeable Battery: A Perspective." *Journal of the American Chemical Society* 135 (2013), pp. 1167–1176.

[19] P. Verma, P. Maire, and P. Novak. "A review of the features and analyses of the solid electrolyte interphase in Li-ion batteries." *Electrochimica Acta* 55 (2010), pp. 6332–6341.

[20] H. Lee, M. Yanilmaz, O. Toprakci, K. Fu, and X. Zhang. "A review of recent developments in membrane separators for rechargeable lithium-ion batteries." *Energy and Environmental Science* 7 (2014), pp. 3857–3886.

[21] L. Croguennec and M. R. Palacin. "Recent Achievements on Inorganic Electrode Materials for Lithium-Ion Batteries." *Journal of the American Chemical Society* 137 (2015), pp. 3140–3156.

[22] M. Winter and J. O. Besenhard. "Wiederaufladbare Batterien, Teil II: Akkumulatoren mit nichtwäßriger Elektrolytlösung." *Chemie in unserer Zeit* 33 (1999), pp. 252–266.

[23] E. Peled. "The Electrochemical Behavior of Alkali and Alkaline Earth Metals in Nonaqueous Battery Systems-The Solid Electrolyte Interphase Model." *Journal of the Electrochemical Society* 126 (1979), pp. 2047–2051.

[24] B. Scrosati, J. Hassoun, and Y. Sun. "Lithium-ion batteries. A look into the future." *Energy and Environmental Science* 4 (2011), pp. 3287–3295.

[25] P. Ramadass Z. Zhang. *Lithium-Ion Battery Systems and Technology*. Ed. by R. J. Brodd. Luxemburg: Springer, 2013.

[26] B. Xu, D. Qian, Z. Wang, and Y. S. Meng. "Recent progress in cathode materials research for advanced lithium ion batteries." *Materials Science and Engineering R* 73 (2012), pp. 51–65.

[27] A. D. McNaught and A. Wilkinson, eds. *IUPAC. Compendium of Chemical Terminology, 2nd ed.* Oxford: Blackwell Scientific Publications, 1990.

[28] K. Mizushima, P. C. Jones, P. J. Wiseman, and J. B. Goodenough. "$Li_xCoO_2(0 < x < -1)$: A new cathode material for batteries of high energy density." *Materials Research Bulletin* 15 (1980), pp. 783–789.

[29] K. M. Shaju, G. V. Subba Rao, and B. V. R. Chowdari. "Performance of layered $Li(Ni_{1/3}Co_{1/3}Mn_{1/3})O_2$ as cathode for Li-ion batteries." *Electrochimica Acta* 48 (2002), pp. 145–151.

[30] Y. Koyama, I. Tanaka, H. Adachi, Y. Makimura, and T. Ohzuku. "Crystal and electronic structures of superstructural Li_{1-x} ($Ni_{1/3}$ $Co_{1/3}Mn$ $_{1/3}$) O_2 ($0 \leq x \leq 1$)." *Journal of Power Sources* 119-121 (2003), pp. 644–648.

[31] N. Yabuuchi and T. Ohzuku. "Novel lithium insertion material of $Li(Ni_{1/3}Co_{1/3}Mn_{1/3})O_2$ for advanced lithium-ion batteries." *Journal of Power Sources* 119-121 (2003), pp. 171–174.

[32] Z. Huang, X. Liu, B. Zhang, S. Oh, P. Ma, and J. Kim. "$Li(Ni_{1/3}Co_{1/3}Mn_{1/3})O_2$ with a novel one-dimensional porous structure: A high-power cathode material for rechargable Li-ion batteries." *Scripta Materialia* 64 (2011), pp. 122–125.

[33] Z. Huang, X. Liu, S. Oh, B. Zhang, P. Ma, and J. Kim. "Microscopically porous, interconnected single crystal $Li(Ni_{1/3}Co_{1/3}Mn_{1/3})O_2$ cathode material for Lithium ion batteries." *Journal of Materials Chemistry* 21 (2011), pp. 10777–10784.

[34] P. Yan, J. Zheng, D. Lv, Y. Wei, J. Zheng, Z. Wang, S. Kuppan, J. Yu, L. Luo, D. Edwards, M. Olszta, K. Amine, J. Liu, J. Xiao, F. Pan, G. Chen, J. Zhang, and C. Wang. "Atomic-Resolution Visualization of Distinctive Chemical Mixing Behaviour of Ni,Co and Mn with Li in Layered Lithium Transition-Metal Oxide Cathode Materials." *Chemistry of Materials* 27 (2015), pp. 5393–5401.

[35] K. Oura, V. G. Lifshits, A. Saranin, A.V. Zotov, and M. Katayama. *Surface Science: An Introduction*. Luxemburg: Springer, 2014.

[36] H. Noh, S. Youn, C. S. Yoon, and Y. Sun. "Comparison of the structural and electrochemical properties of layered $Li(Ni_xCo_yMn_z)O_2$ (x = 1/3,0.5,0.6,0.7,0.8 and 0.85) cathode material for lithium-ion batteries." *Journal of Power Sources* 233 (2013), pp. 121–130.

[37] A. Thaler and D. Watzenig, eds. *Automotive Battery Technology*. Luxemburg: Springer, 2014.

[38] V. Ramadesigan, P. W. C. Northrop, S. De, S. Santhanagopalan, R. D. Braatz, and V. Subramanian. "Modelling and Simulation of Lithium-

Ion Batteries from a Systems Engineering Perspective." *Journal of the electrochemical Society* 159 (2012), R31–R45.

[39] X. Hu, S. Li, and H. Peng. "A comparative study of equivalent circuit models for Li-ion batteries." *Journal of Power Sources* 198 (2012), pp. 359–367.

[40] J. Newman and C. W. Tobias. "Theoretical Analysis of CurrentDistirbution in Porous Electrodes." *Journal of The Electrochemical Society* 109 (1962), pp. 1183–1191.

[41] J. S. Dunning, D. N. Bennion, and J. Newman. "Analysis of Porous Electrodes with Sparingly Soluble Reactants." *Journal of The Electrochemical Society* 118 (1971), pp. 1251–1256.

[42] J. Newman and W. Tiedemann. "Porous-Electrode Theory with Battery Applications." *AIChE Journal* 21 (1975), pp. 25–41.

[43] M. Doyle, T. F. Fuller, and J. Newman. "Modeling of Galvanostatic Charge and Discharge of the Lithium/Polymer/Insertion Cell." *Journal of The Electrochemical Society* 140 (1993), pp. 1526–1533.

[44] C. M. Doyle. "Design and Simulation of Lithium Rechargable Batteries." PhD thesis. Lawrence Berkeley Laboratory - University of California, 1995.

[45] T. F. Fuller, M. Doyle, and J. Newman. "Simulation and Optimization of the Dual Lithium Ion Insertion Cell." *Journal of The Electrochemical Society* 141 (1994), pp. 1–10.

[46] A. Latz, J. Zausch, and O. Iliev. "Modeling of species and charge transport in Li-Ion Batteries based on non-equilibrium thermodynamics" (2010), pp. 329–337.

[47] A. Latz and J. Zausch. "Thermodynamic consistent transport theory of Li-ion batteries." *Journal of Power Sources* 196 (2011), 3296–3302.

[48] K. A. Smith, C. D. Rahn, and C. Wang. "Control oriented 1D electrochemical model of lithium ion battery." *Energy Conversion and Management* 48 (2007), pp. 2565–2578.

[49] Elmer Open Source Simulation Platform. *Elmer Homepage*. 2016. URL: https://www.csc.fi/web/elmer.

[50] Salome Open Source Platform. *Salome Homepage*. 2016. URL: http://www.salome-platform.org.

[51] Paraview Open Source Software. *Paraview Homepage*. 2016. URL: http://www.paraview.org.

[52] K. Fröhlich and A. Trifonova. *Austrian Institute of Technology; Mobility Department*. Private Communication. Website: http://www.ait.ac.at/. 2016.

[53] C. E. Mortimer and U. Müller. *Chemie-Das Basiswissen der Chemie, 8.Auflage*. Stuttgart: Georg Thieme Verlag, 2003.